Molecular simulations of lipid bilayers in interactions with gold nanoparticles

Molekulardynamische Simulationen von Lipid-Doppelschichten in Wechselwirkung mit Gold Nanopartikeln

Master-Thesis von Tobias Pfeiffer aus Heidelberg

Tag der Einreichung: 01.07.2016

1. Gutachten: Prof. Nico van der Vegt
2. Gutachten: Dr. Cahit Dalgicdir

TECHNISCHE UNIVERSITÄT DARMSTADT

Fachbereich Chemie
Center of Smart Interfaces
Computational Physical Chemistry

Molecular simulations of lipid bilayers in interactions with gold nanoparticles
Molekulardynamische Simulationen von Lipid-Doppelschichten in Wechselwirkung mit Gold Nanopartikeln

Vorgelegte Master-Thesis von Tobias Pfeiffer aus Heidelberg

1. Gutachten: Prof. Nico van der Vegt
2. Gutachten: Dr. Cahit Dalgicdir

Tag der Einreichung: 01.07.2016

Erklärung zur Master-Thesis

Hiermit versichere ich, die vorliegende Master-Thesis ohne Hilfe Dritter nur mit den angegebenen Quellen und Hilfsmitteln angefertigt zu haben. Alle Stellen, die aus Quellen entnommen wurden, sind als solche kenntlich gemacht. Diese Arbeit hat in gleicher oder ähnlicher Form noch keiner Prüfungsbehörde vorgelegen.

Darmstadt, den 01. Juli 2016

(Tobias Pfeiffer)

Contents

Abstract

Gold nanoparticles are interesting candidates for medical applications like markers in imaging methods and targeted drug delivery, especially to cancer cells. Unfortunately, many gold nanoparticles have been found to be cytotoxic even for healthy cells. For an application in humans the origin and the factors of this cytotoxicity need to be well understood. In the recent years, many studies have been conducted on nanoparticle cytotoxicity and cellular nanoparticle uptake. Most of them focussed on the penetration of cell membranes and the nanoparticle uptake mechanism. However, there is not much known about the influence of nanoparticles on the properties of intact membranes even though this information is crucial for the assessment of the risk that the use of nanoparticles bears when organisms or the environment are inadvertently exposed to them. The main reason for the lack of knowledge in this field is that there are very few experimental techniques that are able to provide information about the interactions and processes between nanoparticles and cell membranes on the small time and length scales of picoseconds and nanometers. This makes the design of experiments challenging and this is why in this case molecular simulations are a reasonable alternative to experiments. They can provide the information on the small scales in necessary detail to give a better understanding of the general nature of nanoparticle-membrane interactions and to investigate the origin of effects seen in experiments. In this work, coarse-grained molecular simulations were used to investigate the influence of small alkanethiolate-coated gold nanoparticles on the properties of lipid bilayers as a model for cell membranes.

In the simulations three different lipid bilayers in water consisting of pure 1-palmitoyl-2-oleoyl-sn-glycero-3-phosphocholin (POPC), pure 1-palmitoyl-2-oleoyl-sn-glycero-3-phospho-(1'-rac-glycerol) sodium salt (POPG) and a mixture of the two in molar ratio 1:1 were used. Both lipids are monounsaturated and identical in structure except for their head groups. POPC has a zwitterionic neutral head group, while POPG has a negative one. Additionally, two different gold nanoparticles, one with a positively and one with a negatively charged coating were used. The gold cores of both nanoparticles consisted of 79 gold atoms in the shape of a truncated octahedron with 38 alkanethiolate chains connected to the surface via their sulphur atoms. The gold core had a diameter of 1.2 nm while the diameter with the coating was around 4 nm. The MARTINI model was used for the simulations, which maps 4 heavy atoms into one single interaction site. This coarse-graining made the necessarily long time and length scales of the simulations accessible while preserving the relevant chemistry of the systems. All simulations featured a lipid bilayer in water in the middle of the simulation box with one or more nanoparticles placed in the water above the bilayer. Simulations of the bilayers in the absence of nanoparticles were used for model validation and as a reference for unperturbed membranes.

Small systems with 10×10 nm bilayer patches with all six possible combinations of the two nanoparticles and three lipid bilayers were used to investigate nanoparticle attachment to the membranes. They showed that electrostatic interactions are guiding the nanoparticle attachment on the lipid bilayers and that there is a weaker and a stronger state of attachment. In the weaker state the head groups of the lipids are in contact with the ligand coating while they are in contact with the sulphur atoms and the gold core in the stronger binding state. The stronger binding state was reached via the metastable weaker one and only for the cationic nanoparticle on the two negatively charged bilayers (POPC/POPG and POPG).

Bigger simulations with 40×40 nm membrane patches and four or 16 nanoparticles were used to investigate the influence of the nanoparticles on the structural properties of the bilayers. The nanoparticles perturbed the density profiles of the bilayers and reduce dlipid order in their close neighborhood, but only in the lipid layer facing them. The influence is stronger for the stronger binding states. The opposing lipid layer was almost unaffected. However, no influence of the nanoparticles on the area per lipid or the membrane thickness was observed. The calculation of radial distribution functions showed that the nanoparticles changed the local composition of the mixed bilayer due to a preference of POPG over POPC in contact with the nanoparticles. This demixing also causes the nanoparticles to form dynamic structures on the membrane surface, in which the average distance between the nanoparticles is reduced. It remains unclear if this is the clustering of nanoparticles on membranes observed in experiments.

The simulations with 16 nanoparticles also showed that nanoparticles reduce the lateral motion of lipids in the bilayer globally and on a molecular level. This has previously been observed in experiments and a formation of lipid-rafts under the nanoparticles was proposed as a possible explanation. The simulations were able to show that lipids close to nanoparticles tend to bind to them for a longer time and therefore diffuse with a reduced rate. However, the raft-like domains around the nanoparticles are not rigid but instead dynamic structures with a steady exchange of lipids between the raft and its surrounding. Summarizing, the simulations were not only able to reproduce the experimental results and effects but also to give insights in the underlying processes that have not yet been observed in experiments.

Zusammenfassung

Gold Nanopartikel sind vielversprechende Kandidaten für verschiedene Anwendungen in der Pharmazie. Dazu zählen deren Einschleusung in und der gezielte Transport von Medikamenten zu bestimmten Zellen, wie zum Beispiel Krebszellen, aber auch deren Nutzung als Kontrastmittel in bildgebenden Verfahren und der *in vivo*-Spektroskopie. Dabei macht man sich zu Nutze, dass metallische Nanopartikel in der Lage sind Zellmembranen zu durchdringen. Diese Eigenschaft macht Nanopartikel jedoch oft auch cytotoxisch für gesunde Zellen. Viele Studien der letzten Jahre haben deshalb die verschiedenen Faktoren in der Struktur der Nanopartikel untersucht, die für die Durchdringung oder Zerstörung von Zellmembranen relevant sind. Man hofft die Cytotoxizität der Nanoteilchen damit schon bei der Synthese kontrollieren zu können. Während der Mechanismus für die Aufnahme der Nanopartikel in die Zellen vielfach untersucht wurde, ist nur sehr wenig bekannt über die generellen Einflüsse, die Nanoteilchen auf Membranen haben können ohne sie zu durchdringen oder zu zerstören. Dieses Wissen ist jedoch dringend erforderlich, wenn Gold Nanopartikel medizinisch angewendet werden sollen, da man sonst nicht abschätzen kann, welches Risiko bei unbeabsichtigter Exposition für den Patienten, aber auch für andere Organismen und die Umwelt besteht. Einer der Hauptgründe für den Mangel an Untersuchungen in diesem Feld ist, dass es bisher nur wenige experimentelle Techniken gibt, mit denen sich die entscheidenden Prozesse auf Nanometer- und Picosekundenskalen untersuchen lassen. Eine gute Alternative dazu stellen molekulardynmaische Simulationen dar, die in der Lage sind auf kurzen Zeit und Längenskalen detaillierte Informationen zu liefern. In der vorliegenden Arbeit wurden deshalb Simulationen von verschiedenen Lipid-Doppelschichten, als Modell für Zellmembranen, in der Anwesenheit von Thiolalkan-ummantelten Gold Nanopartikeln durchgeführt und der Einfluss der Nanopartikel auf statische und dynamische Membraneigenschaften untersucht.

Für die Simulationen wurde das MARTINI-Modell verwendet. Dieses ist ein vergröbertes Modell, in dem jeder Partikel vier schwere (nicht-Wasserstoff) Atome repräsentiert. Diese Vergröberung war notwendig um die verwendeten Systemgrößen und Simulationszeiten zu erreichen. Das MARTINI Model ist jedoch in der Lage, trotz des Verlustes atomistischer Details, die relevante Chemie der simulierten Systeme zu erhalten. Vor allem Lipide sind im MARTINI-Modell sehr gut parametrisiert und zeigen alle relevanten Phasen in Wasser. Dies war, zusammen mit der Tatsache, dass auch ein Modell für Gold Nanopartikel aus einem vorherigen Projekt bereits verfügbar war, der Hauptgrund für die Wahl dieses Modells. Die beiden verwendeten Lipide, 1-palmitoyl-2-oleoyl-sn-glycero-3-phosphocholin (POPC) und 1-palmitoyl-2-oleoyl-sn-glycero-3-phospho-(1'-rac-glycerol) (POPG), zweiteres verwendet als Natriumsalz, wurden durch jeweils 12 Partikel repräsentiert. Diese beiden einfach ungesättigten Lipide sind bis auf die Kopfgruppen identisch. POPC hat eine zwitterionische und damit neutrale Kopfgruppe, während POPG eine negative Ladung an der Kopfruppe aufweist. Die Nanopartikel haben einen Kern aus 79 Goldatomen in Form eines Oktaederstumpfes, an dessen Oberfläche 38 Dodecanylreste über jeweils ein Schwefelatom gebunden sind. Im MARTINI-Modell wird dies durch einen Partikel für jedes Gold- und Schwefelatom sowie durch einen Partikel für jede Vierergruppe von Kohlenstoffatomen dargestellt. Der Durchmesser des Goldkerns betrug 1,2 nm, der Gesamtdurchmesser mit Ummantelung ca. 4,0 nm. Um verschiedene Ladungen in der Ummantelung der Nanopartikel zu untersuchen, wurde das letzte Kohlenstoffteilchen in der Kette mit entweder einer positiven oder einer negativen Ladung versehen. Dies resultierte in einem Modell für einen kationischen und einem anioischen Nanopartikel.

In den Simulationen wurden drei verschiedene Lipid-Doppelschichten , bestehend aus POPC, POPG und POPC/POPG im molekularen Verhältnis 1:1, in Wasser in unterschiedlichen Größen in Präsenz von einem oder mehreren Nanopartikeln untersucht. Simulationen von Membranen ohne Nanopartikel wurden zur Validierung des Membranmodells und als Referenz verwendet. Die Lipid-Doppelschicht wurde jeweils in der Mitte der Simulationsbox platziert, während die Nanopartikel in das Wasser darüber mit einem Abstand von 5–8 nm zur Membran gesetzt wurden. Die Referenzsysteme ohne Nanopartikel zeigten, dass die Struktur der Membranen in den Simulationen in Einklang mit experimentellen Messdaten war. Dies gilt vor allem für die Fläche pro Lipid, die Dicke der Doppel-Lipidschicht und das Dichteprofil. Außerdem wurde gezeigt, dass die Membranen, wie gewünscht, keine Oberflächenspannung haben.

Das generelle Verhalten der Nanopartikel-Membran-Systeme wurde in kleinen Simulationen untersucht. Dabei wurde in einer $10 \times 10 \times 25$ nm Simulationsbox ein Nanopartikel über einer 10×10 nm Lipidmembran platziert und das System für eine Gesamtzeit von 2 μs simuliert. Dabei wurden alle drei Lipidschichten mit jeweils einem positiv oder einem negativ geladenen Nanopartikel kombiniert. Die Simulationen der sechs verschiedenen Kombinationen zeigten, dass Coulomb-Wechselwirkungen entscheidend für die Herstellung eines stabilen Kontaktes zwischen Nanopartikel und Membran sind. So banden sich die kationischen Nanopartikel schnell an die Membranen mit negativer Oberflächenladung (POPG und POPC/POPG), während die anionischen Nanopartikel durch Abstoßungskräfte daran gehindert wurden. In Wechselwirkung mit der neutralen POPC Membran zeigten die Partikel wie erwartet identisches Verhalten. Des Weiteren

konnten zwei unterscheidlich starke Bindungszustände der Nanoteilchen an den Membranen beobachtet werden. Im schwächeren der beiden Zustände befinden sich die Kopfgruppen der Lipide in Kontakt mit den Kopfgruppen der Ummantelung der Nanopartikel, im stärkeren in Kontakt mit den Schwefelatomen und dem Goldkern. Der stärkere wurde in den Simulationen immer über den metastabilen schwächeren Bindungszustand erreicht.

Simulationen größerer Systeme mit 40 × 40 nm Membranstücken mit jeweils vier oder 16 Nanoteilchen zeigten den Einfluss der Nanopartikel auf verschiedene Membraneigenschaften. So verändern Nanopartikel das Membranprofil in ihrer Umgebung, vor allem, wenn sie stark gebunden sind. Schwächere Bindungszustände beeinflussen das Membranprofil kaum. Des Weiteren konnte gezeigt werden, dass die Ordnung der Lipide in der Membran in der Umgebung der Nanopartikel stark abnimmt. Dies gilt jedoch nur für die Lipidschicht in direktem Kontakt mit den Nanoteilchen. Die gegenüberliegende Lipidschicht blieb in all ihren Eigenschaften nahezu unbeeinträchtigt. Auch konnte keinerlei Veränderung der Fläche pro Lipid, der Dicke der Lipid-Doppelschicht oder der Oberflächenspannung durch die Nanopartikel beobachtet werden.

In der Simulation der gemischten Lipid-Doppelschicht wurde die lokale Zusammensetzung durch die Nanopartikel verändert. Dies konnte durch Berechnung der radialen Verteilung der unterschiedlichen Lipide um die Nanopartikel auf der Membran gezeigt werden. Diese lokale Entmischung der Lipide wird verursacht durch die höhere Affinität von POPG gegenüber POPC in Kontakt mit den positiv geladenen Nanoteilchen. Die induzierte lokale Entmischung sorgt dann wiederum dafür, dass sich die Nanoteilchen auf der gemischten Membran anders verhalten als auf den Membranen mit nur einer Komponente. Sind die Nanopartikel auf der POPG Membran noch nahezu gleichmäßig verteilt, so bilden sie dynamische Strukturen mit geringerem Abstand zwischen den Nanopartikeln auf der POPC/POPG Membran. Dies konnte durch Berechnung der radialen Verteilung von Nanopartikeln umeinander gezeigt werden. Ob es sich dabei um die in Experimenten beobachteten Nanopartikel-Cluster handelt, die sich auf Lipidmembranen bilden können, konnte nicht abschließend geklärt werden.

Zuletzt wurde die laterale Diffusion von Lipiden in der Membran in der Anwesenheit von Nanopartikeln untersucht. Dies zeigte, dass Nanopartikel sowohl die globalen Diffusionsraten von Lipiden in der Membran reduzieren, als auch die Verteilung der molekularen Diffusionskoeffizienten beeinflussen. Dies ist zwar zuvor in Experimenten beobachtet worden, jedoch konnte in dieser Arbeit erstmals die Ursache dieses Effektes identifiziert werden. Die Beobachtung einzelner Lipide und Nanoteilchen in den Simulationen zeigte, dass Lipide über größere Zeitintervalle an einzelne Nanopartikel binden und zusammen mit diesem entlang der Membranoberfläche diffundieren. Diese Bindung ist jedoch reversibel und es gibt einen stetigen Austausch zwischen der an den Nanopartikel gebundenen Lipide mit der Umgebung. Dies bestätigt den aus den Experimenten vermuteten Mechanismus der Bildung von Lipid-Flößen unter den Nanoteilchen, zeigt jedoch auch, dass diese Strukturen nicht fest, sondern viel dynamischer sind als zuvor angenommen.

Zusammenfassend konnte in dieser Arbeit gezeigt werden, dass die Simulationen gut zur Untersuchung der betrachteten Modellsysteme geeignet sind, da sie die experimentellen Ergebnisse reproduzieren und gleichzeitig neue Einblicke in die Wechselwirkungen und Prozesse zwischen Nanoteilchen und Lipidmembranen geben konnten.

1 Introduction

Inorganic nanoparticles (NPs) have been in the focus of research for the last 20 years. With their size they build a connection between atomic and bulk properties. For example they show a higher reactivity due to their high surface area per volume and their spectra are dominated by size effects, making them quantized. All this makes them highly interesting for many applications especially in spectroscopy, where they can be used as markers[1,2], materials science, where they modify the properties of polymers[3] and pharmacology, where the number of applications has steadily grown.[4] There are two main fields of medical applications of nanoparticles: NPs with different optical properties for use as imaging agents (*e.g.* gold NPs whose color can be adjusted by their size[5], quantum dots that have fluorescent properties[6] and superparamagnetic iron oxide nanoparticles for use in magnetic resonance imaging of cancer tumors[7]) and NPs that are used for targeted drug delivery to cells. Examples of the latter are coated gold nanorods that transport the drug in their protein corona for triggered release[8] and the thermal destruction of cancer cells using the plasmon resonance of gold nanoparticles[9,10]. One of the biggest problems in these applications is the cytotoxicity of nanoparticles, as they have shown to penetrate or disrupt cell membranes even of healthy cells.[11]

However, while there are already medical applications for nanoparticles in humans, there are still many things unknown about the behavior of these materials in biological environments. Especially the interactions of nanoparticles and membrane surfaces are still being investigated, but without this knowledge, it is impossible to determine the long-term effects of nanoparticles and risks for humans, the ecosystem and the environment in these applications. Many studies have been performed to investigate the influence of different parameters, such as size, shape and NP coating on the cytoxicity and cellular uptake of nanoparticles. The final goal of these studies is understanding the causes and mechanisms of the NPs to control these effects and make nanoparticles "safe-by-design".[12–16] While there are some first insights about this, very little is known about the interactions of inorganic nanoparticles attached to membranes without penetration or disruption. Especially the influence of attached nanoparticles on the membrane properties is hardly investigated. This information, however, is crucial for the design of non-cytotoxic nanoparticles.

Montis *et al.* recently reported that gold nanoparticles form agglomerated structures in the colloidal domain and at the same time reduce the diffusion rates of lipids in the molecular domain on giant unilamellar vesicles. These are often used as membrane models in experiments. For the latter effect they proposed a mechanism of enslaved diffusion, in which the lipids in contact with the nanoparticles form raft-like structures. They also emphasized the importance of a multi-scale approach for the investigation of these effects.[17]

The main reason for the lack of further information on this topic is that the observations must be made on a nanoscale, which reduces the number of possible techniques and thus makes the design of experiments very challenging. This is where investigations with molecular simulation techniques are a useful tool. They provide detailed insights on the effects and processes at the nanoparticle-membrane interface in atomistic or at least molecular resolution that can hardly be matched by experiments. However, it is difficult to model biosystems in molecular simulations due to their complexity. Cellular membranes consist of a mixture of different phospho- and sphingolipids, sterins, membrane proteins and other components.[18] Therefore, model membranes are normally used in molecular simulations to avoid the necessity of a realistic representation of the cell membranes. With this approach the general behavior of membrane systems can be investigated as has been done in this work. These simulations may not be directly comparable with *in vitro* experiments but they can provide relevant information about the general nature of the structural and dynamic changes of the membranes, as long as all the necessary physical interactions are considered in the model. Several simulation studies of systems containing lipid membranes and nanoparticles have been performed in the last years but, like the experimental studies, the majority of them focussed on the penetration or disruption of the membrane by the nanoparticles.

Gkeka *et al.* performed two studies on the uptake mechanism of nanoparticles into lipid bilayers. The first one focussed on the influence of the surface pattern of spheric nanoparticles on the free energy profile of the peentration of the lipid bilayer.[19] It showed that a homogeneous pattern dramatically enhances permeation and that ligands in their simulations rearranged themselves in a manner that provided these patterns, even if they were initially arranged differently. The second study investigated the structure of nanoparticles that were inserted into a bilayer consisting of DPPC and cholesterol.[20] These final configurations showed a snorkeling effect, that removed the negative ligand head groups from the middle of the bilayer and pushed them to the bilayer surfaces. This configuration minimizes the coulomb energy as the charged ligand head groups are in close contact with the lipid head groups.

Simonelli *et al.* investigated the mechanism of the insertion of coated, anionic gold nanoparticles into a lipid bilayer in a study similar to the ones of Gkeka *et al.*.[21] They reported a three-staged process in which the nanoparticle is adsorbed on the membrane, then establishes a hydrophobic contact with the tails of the upper lipid layer and then rearranges the ligand tails, so that they interact with the head groups of the opposing lipid layer, one at a time. They also show that the surface pattern of the nanoparticle, *i. e.* the arrangement of different ligands on the surface of the nanoparticle core, has an influence on the free energy profile of the insertion. Nanoparticles with a randomized surface pattern experience a lower energy barrier than nanoparticles with the different ligands arranged in a striped pattern.

Heikkilä *et al.* conducted a study on the binding of cationic and anionic alkylthiolate-coated gold nanoparticles on plasma membrane like lipid bilayers using atomistic molecular dynamics.[22,23] These simulations showed different affinities of the nanoparticle to the bilayer in the intra- and the extracellular compartments. They were also able to analyze the changes in the structure of the nanoparticles and the membranes caused by the attachment. In this way, it could be shown that the nanoparticle pushes the lipid head groups aside, when it gets in close contact to the bilayer. This was interpreted as a first step of an insertion of the nanoparticle into the membrane.

A study on the influence of uncoated gold nanoparticles of different sizes on the properties of a lipid bilayer by Mhashal *et al.* used a united atom model.[24] They reported a decrease in lipid order and lipid diffusion rates. A weakness of this study is that the systems are very small and also the nanoparticle model is not representative, but the main problem is the overall poor quality of the work.

Lin *et al.* performed coarse-grained simluations of alkanethiolate-coated gold nanoparticles with a diameter of 2 nm on lipid bilayers consisting of DPPC and DPPG using the MARTINI model. They investigated the importance of electrostatic interactions on the attachment and insertion of nanoparticles into the bilayer. Therefore they simulated gold nanoparticles with cationic, neutral and anionic alkythiolate coatings on DPPC and DPPC/DPPG membranes. Their results showed that electrostatic attraction is crucial for the binding of nanoparticles to lipid bilayers.[25] Also they were able to show the formation of holes on a small bilayer patch caused by an insertion of the nanoparticle into the bilayer.[26] They were even able to observe the penetration of a membrane by a nanoparticle in the presence of a strong transmembrane potential, in which the bilayer temporarily formed an opening to make room for the nanoparticle.[27]

Besides classical molecular dynamics, there is a study by Curtis *et al.* who investigated the influence of the nanoparticle size on if a nanoparticle is translocated into or wrapped by a membrane using discontinuous molecular dynamics[28]. Another study of Tian *et al.* used dissipative particle dynamics to show different reactions of membranes to contact with nanoparticles, from attachment over wrapping to disruption, but were not able to provide new insights on this topic[29].

All previously published studies have in common that systems of minimal size have been used, that no more than one nanoparticle was present in the simulations and that the simulation times have not been particularly long. The latter one is surprising considering that many of them report long time scales for the observed processes.

The goal of this work was the investigation of the influence of alkylthiolate coated nanoparticles on the static and dynamic properties of lipid bilayers using coarse-grained molecular dynamics. The focus was on a better understanding of the general processes in these model systems rather than the replication or prediction of experimental results. However, the simulated systems were chosen to be compared with experimental data. This mainly involves larger systems, with a high number of particles, and the simulation of systems containing multiple nanoparticles. As such simulation studies have not been performed before, they could provide new insights in the interactions of nanoparticles and membranes.

2 Model

This section describes the model used for the simulations in this work. In subsection 2.1, a quick overview of the concepts and features of the MARTINI model is given as this information is important for the introduction of the lipid and nanoparticle models in subsections 2.2 and 2.3 as well as for the assessment and discussion of the results in section 4.

2.1 The MARTINI model

The MARTINI model developed by Marrink *et al.* [30,31] is a coarse-grained model for molecular dynamics. It generally uses a 4:1 mapping of heavy atoms (C, N, O, ...*etc.*) including all hydrogen atoms bound to them. It uses 4 general types of interactions sites instead of specific representations for every possible group. The four basic bead types are polar (P), nonpolar (N), apolar (C), and charged (Q), which have 4 or 5 subtypes to account for differences in polarity or the ability to form hydrogen bonds. Polarity ranges from 1 = low to 5 = high, while for the hydrogen bonding a = acceptor, d = donor, da = donor and acceptor, 0 = none are used. By default all interaction sites have the same mass of 72 atomic mass units (corresponding to the weight of four water molecules). The small number of different bead types and interactions makes this model very simple yet ensures that the chemistry of the systems is represented.

Two kinds of nonbonded interactions between beads at a distance r are considered in the MARTINI model. Lennard-Jones 12-6 potentials $U_{LJ}(r)$ (see equation 2.1) are used for all interactions that are not electrostatic. With very few exceptions the same effective size is used for all beads with $\sigma = 0.47$ nm. In total there are 10 different levels of interactions numbered, with roman numerals from 0 to IX, with 10 corresponding values of the potential depth ϵ ranging from 2.0 kJ mol^{-1} to 5.6 kJ mol^{-1}. Again, this makes it possible to adjust interactions to fit experimental values with a low number of different interaction strengths.

$$U_{LJ}(r) = 4\epsilon_{ij}\left[\left(\frac{\sigma}{r}\right)^{12} - \left(\frac{\sigma}{r}\right)^{6}\right] \tag{2.1}$$

Charged groups additionally interact using a shifted Coulomb potential $U_C(r)$ (equation 2.2) with electric charges q_i and q_j, dielectric constant ϵ_0 and distance r. Some parts of the electrostatic interactions are actually parametrized in the Lennard-Jones potentials of the van-der-Waals inteactions. Ions in the MARTINI model are considered with their first hydration shell included in the ion bead, but with full charges. The relative dielectric constant ϵ_r is set to 15 in water. This leads to an overestimation of the electrostatic interactions in the MARTINI model. However, this was accepted as for the simulation of a model system, perfect balance of all interactions was not considered very important, especially because there are no experimental data to parametrize all the other interactions of the nanoparticle adequately.

$$U_C(r) = \frac{q_i q_j}{4\pi\epsilon_0\epsilon_r r} \tag{2.2}$$

Bonded interactions are included as harmonic potentials for bonds $V_B(R)$ (equation 2.3) and angles $V_A(\theta)$ (equation 2.4). Herein R denotes the distances between the bonded interaction sites, k_B the harmonic bond constant and R_0 the equilibrium distance of the bond while analogously θ denotes the angle between two neighboring bonds, k_A denotes the harmonic constant for the angle and θ_0 denotes the equilibrium angle between the two bonds. Standard values used in the MARTINI model are: $R_0 = \epsilon = 0.47$ nm, $k_B = 1250$ kJ mol^{-1}nm^{-2}, $\theta_0 = 180°$ and $k_A = 25$ kJ mol^{-1}. However, these may be changed to get a better description of the structure of the system.

$$V_B(R) = \frac{1}{2}k_B\,(R - R_0)^2 \tag{2.3}$$

$$V_A(\theta) = \frac{1}{2}k_A\,(\cos\theta - \cos\theta_0)^2 \tag{2.4}$$

The MARTINI model makes use of an explicit solvent model, in which water interaction sites each represent four water molecules. The water model used was not polarizable. The water density is 0.99 g cm^{-3} and the freezing point is at 290 ± 5 K. However, spontaneous freezing is not observed until a temperature of 240 K, except in the presence of other

rigid surfaces or objects in contact with water that initialize the freezing process.[30] The self-diffusion coefficient of water has been reported as $D_W = 5\times10^{-6}\mathrm{cm}^2\mathrm{s}^{-1}$. To account for the fact that the water beads actually represent four water molecules instead of one, this value has to be multiplied with a factor of four[32], resulting in a diffusion coefficient of $D_w = 2\times10^{-5}\mathrm{cm}^2\mathrm{s}^{-1}$ for a single molecule. This value is usually compared to experimental data, to estimate a factor for the conversion of dynamic quantities from the coarse-grained simulation to reality. The experimental value for the self-diffusion of water at 293 K is $D_{ex} = 2.3\times10^{-5}\mathrm{cm}^2\mathrm{s}^{-1}$.[33] Therefore, there would not be any acceleration of the dynamics in the MARTINI simulations after consideration of the mapping scheme. However, this is only the case for the time step of 50 fs that was chosen by Marrink *et al.* for these investigations. A reduction of the time step in the simulations has a strong influence on the self-diffusion coefficient of the water beads and also smaller time-steps are explicitly recommended for the use of the MARTINI model. Marrink *et al.* suggest a general conversion factor of 3-4, which is in agreement with the diffusion rates of the water molecules at smaller time-steps below 50 fs and thus has been used for the conversion of dynamic quantities in this work.

The MARTINI model was chosen for the use in this work because it provided the necessary reduction of interaction sites, to access the large time and length scales in the simulations, while preserving the chemistry of the systems. The main reason, however, was that models for lipids and nanoparticles were already available in good quality. The MARTINI model provides representations and force-field parameters for a wide range of lipids, that are able to reproduce many different phases, including bilayers in water. The nanoparticle model, on the other hand, has been developed by the author previously to this work.

2.2 Nanoparticle model

In the following subsection 2.2 the model of the nanoparticle is introduced. It has been developed in a research project prior to the work related to this thesis. As there are no publications on it at the time this thesis is written, the following section has completely been taken from the report on mentioned research project. The following paragraph describing the general properties is a summary, leaving out details of the decisions and development process that are not important in the context of this work. The following part of this subsection, which describes the model parameters, has been taken from the report without any changes.

The nanoparticles used in the simulations consist of a gold core which is coated by alkylthiolate ligands. The gold core is build up of 79 gold atoms forming a truncated octahedron with two different surfaces ([111] on the former octahedron faces and [001] where the octahedron was truncated) on a face-centered cubic lattice. The medium diameter of the gold core is 1.2 nm. 38 dodecane thiol ligands are connected to the surface of the gold core via their sulphur atoms. The last carbon atom of the dodecane thiol ligands was replaced by either an ammonia or a carboxylate group to create cationic or anionic coatings for the nanoparticles, respectively (see figure 2.1a). In the work related to this thesis the neutral coating has not been used.

The dodecanthiol chains are mapped using four beads: One bead for the sulphur atom connecting the carbon chain to the gold nanoparticle, followed by three beads that each represent a segment of four carbon atoms of the dodecanyl substituent. In the nanoparticles with charged ligands the last bead represents three carbon atoms with an ammonia or carboxylic goup at the end. This is shown in figure 2.1b.

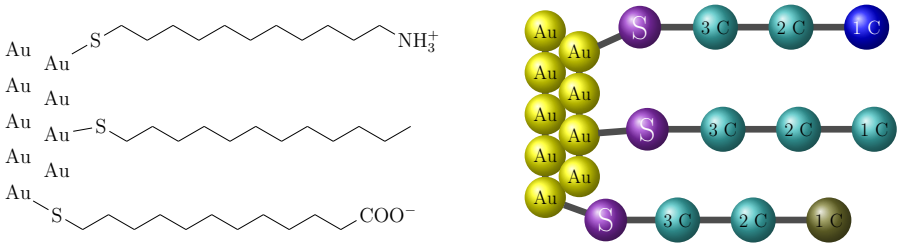

(a) structural formula **(b)** MARTINI representation

Figure 2.1: Structures of the nanoparticle surface with a cationic (upper), a neutral (middle) and an anionic (lower) dodecane thiol ligand.

The bead type assignment was taken from Lin *et al.*.[26] However the mass of the gold beads was increased to 196.0 atomic mass units to take into account the significantly higher mass of the gold atoms and to model a diffusion behaviour closer

to reality. Table 2.1 shows the bead types from the MARTINI model assigned to the beads used in the simulations together with their masses and charges.

Table 2.1: Beads used in the simulation with their MARTINI types, masses and charges.

Bead name	**MARTINI type**	**Mass** [u]	**Charge** [e]
W	P4	72.0	0.0
NA+	Qd	72.0	+1.0
CL-	Qa	72.0	-1.0
Au	C5	196.0	0.0
S	N0	72.0	0.0
3C	C1	72.0	0.0
2C	C1	72.0	0.0
1C	Qa C1 Q0	72.0	+1.0 0.0 -1.0

The intermolecular interaction potentials from the MARTINI model were used without any changes. For the modelling of the intramolecular interactions, harmonic potentials were used for bonds and angles. Thereby the interactions between gold atoms in the core were modelled with harmonic potentials taken from Milano *et al.*[34], while all other harmonic bond and angle potentials in the nanoparticle model were taken from Lin *et al.*.[26] The reasons for the use of a non-rigid model of the gold core are prevention of spontaneous water freezing due to a contact with a solid surface and reduction of the computational effort, as harmonic potentials are cheaper than constraint algorithms. All bond and angle types occurring in the nanoparticle, together with their equilibrium distances/angles (R_0 or θ_0) and their harmonic force constants (k_B or k_A, respectively), are listed in table 2.2. There are three equilibrium distances for the Au-Au bond for the different distances between neighboring atoms in the truncated octahedron.

Table 2.2: Bond and angle potentials of the different gold nanoparticles.

Bond	**Distance** R_0 [nm]	**Force constant** k_B [kJ mol^{-1}nm^{-2}]
Au-Au	0.2924	50000
	0.2920	50000
	0.2917	50000
Au-S	0.2400	6400
S-C3	0.4700	1250
C3-C2	0.4700	1250
C2-C1	0.4450	1250
Angle	**Angle** θ_0 [°]	**Force constant** k_A [kJ mol^{-1}rad^{-2}]
S-C3-C2	180	25
C3-C2-C1	180	25

2.3 Membrane model

Two different lipids are used to build up membranes in the simulations: 1-palmitoyl-2-oleoyl-sn-glycero-3-phosphocholine (POPC) and 1-palmitoyl-2-oleoyl-sn-glycero-3-phospho-(1'-rac-glycerol) (sodium salt) (POPG). These lipids were chosen to make the results of the simulations comparable to the experimental data of Montis *et al.*.[17] Also both of these lipids are relevant components in mammalian cell membranes, which makes the resulting bilayers good models of biological membranes.[35] Both lipids have one oleic acid tail, which has a double bond in the middle, and a palmitic acid tail, which is completely saturated. With a zwitterionic phosphocholine head group, POPC is a neutral

lipid. On the other hand the head group of the POPG molecule only carries one negative charge at the phosphate group. The second, outermost part of the lipid head is uncharged, yet hydrophilic due to two hydroxy groups on the last two carbon atoms. As in experiments, the sodium salt of POPG is used in the simulations. The use of one negative and one neutral lipid enables a tuning of the negative surface charge of the lipid bilayer, which is useful because it is an important property of most mammalian cell membranes.

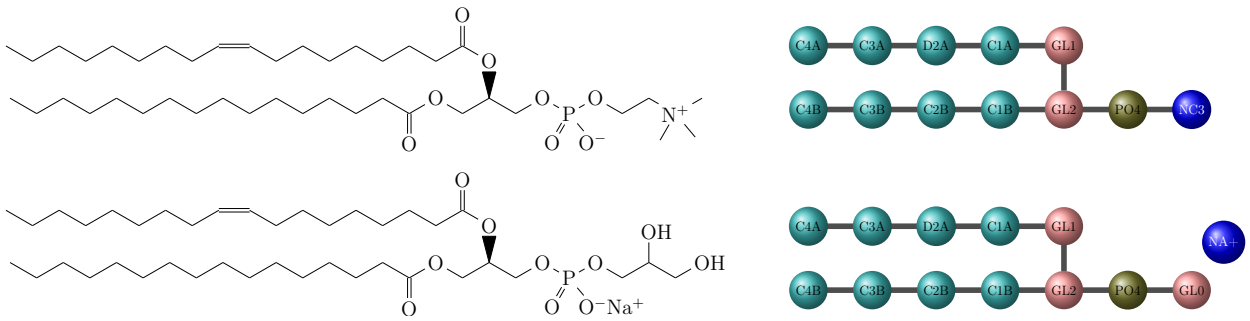

(a) structural formulas **(b)** MARTINI representation

Figure 2.2: Structural formulas and coarse-grained representations of POPC (top) and POPG (bottom).

Figure 2.2 shows the structural formulas and the corresponding official representations version 2.0 in the MARTINI model for the two lipids.[30,31,36,37] Therefore the bead type assignments and intramolecular interactions are not tabulated here. In the coarse-grained model, the lipid tails are represented by four beads, each representing 4 carbon atoms, with names C1A, D2A, C3A, C4A and C1B to C4B. Thereby the first letter of the name marks the bead as saturated (C) or unsaturate (D) carbon. The number stands for the position in the carbon chain and the last letter gives information about which of the two tails the bead belongs to. Carbon beads with names ending on an "A" belong to the palmitic acid tail, while carbon beads with names ending on an "B" belong to the oleic acid tail. The beads named GL1 and GL2 connect the lipid tails with the the two head group beads named PO4 and NC3 or GL0 for POPC and POPG, respectively.

3 Simulations

The computations for this work have been performed on the following supercomputers: Lichtenberg-Hochleistungrechner at the Technische Universität Darmstadt, GALILEO supercomputer of CINECA in Bologna and GASPARRI at the Università degli studi di Salerno.

3.1 Software and analysis

For all simulations and trajectory analysis GROMACS version 5.1.1 was used.[38–44] The systems were prepared using Packmol version 15.217.[45] For visualization VMD version 1.9.2 was used.[46] Graphs were produced with Grace version 5.1.22, GNUplot version 5.0 or OriginPro version 8.0

Trajectories were analyzed with the following GROMACS tools: `gmx analyze`, `gmx density`, `gmx energy`, `gmx angle`, `gmx distance`, `gmx msd`, `gmx order` and `gmx rdf`. Additionally, the provided GROMACS C++ template for costumized analysis tools has been used to write new analysis tools: `localorder` and `fractions`. The program code for the latter ones are included in the appendix. A short description of their basic algorithms is given in subsection 4.2.3.

3.2 Systems

In the work related to this thesis, four general types of systems have been simulated:

- a big membrane patch without nanoparticles
- a small membrane patch with 1 nanoparticle
- a big membrane patch with 4 nanoparticles
- a big membrane patch with 16 nanoparticles

For each system type several simulations with different compositions of the lipid bilayer and nanoparticle types have been performed. With each stage, more and more of these combinations have been relinquished as they did not show the desired behavior for the following investigations. Details on the choice of the systems in the different stages of the investigations can be found in section 4. The following subsection describes the four general system types and lists the different simulations together with their exact compositions.

In the first stage, lipid bilayer patches surrounded by water have been simulated. These simulations have been used as a reference for the behaviour of the unperturbed membranes. A total of three different lipid compositions was used to build up the membranes: pure POPC, pure POPG and a mixture of them with a molar ratio of 1:1. Each membrane patch had a size of approximately 40×40 nm with $\sim$10 nm of water below and above the bilayer, resulting in an approximately $40 \times 40 \times 25$ nm simulation box. Each lipid layer consisted of around 2500 lipids in accord with the experimental surface areas per lipid for the corresponding lipids.

Simultaneously, smaller systems were simulated to investigate the general behavior of the different combinations of nanoparticles on lipid bilayers. A 10×10 nm patch of the three bilayers (POPC, POPG, POPC/POPG) were simulated with either one cationic or one anionic nanoparticle with counterions. The box height was kept at 25 nm. In the resulting 6 systems the nanoparticles were placed at a distance of 5 nm from the bilayer to see if they would attach to the membrane or not. The total number of lipids in these simulations was around 300, with 150 lipids in each layer.

The promising combinations of nanoparticles and lipid bilayers, which showed a strong attachment, were chosen based on the behavior of the small systems. These were all the systems that included the positively charged nanoparticles. The next stage of simulations featured the big membrane patches from the first stage to which 4 cationic nanoparticles each were added. The goal of the simulations was the investigation of the general nature of the nanoparticle interactions on the lipid bilayer and to see if the global properties of the bilayer would be influenced at lower nanoparticle concentrations.

In the last stage of this work the number of nanoparticles on the lipid bilayer was increased to investigate the influence of the concentration, but also to get better statistics due to an increased sample size. 16 cationic nanoparticles were placed

on one side of the 40 × 40 nm lipid bilayers in each simulation. However, only the two negatively charged membrane patches (POPG and POPC/POPG) have been used, as the influence of the nanoparticles on the neutral POPC bilayer were considered too weak after the third stage.Table 3.1 lists the systems simulated in the four different stages with their system sizes and numbers of all the molecules.

Table 3.1: System sizes in nm and numbers of molecules (beads for water and ions) of the simulations in the four stages.

Stage	Membrane	Size in nm($x \times y \times z$)	POPC	POPG	NP cationic	NP anionic	Water	Na^+	Cl^-
1	POPC	40 × 40 × 25	5396	0	0	0	285734	0	0
	POPG		0	4864	0	0	260736	4864	0
	Mixture		2560	2560	0	0	263040	2560	0
2	POPC	10 × 10 × 25	338	0	1	0	19382	0	38
			338	0	0	1	19382	38	0
	POPG		0	304	1	0	17956	304	38
			0	304	0	1	17956	342	0
	Mixture		160	160	1	0	18501	160	38
			160	160	0	1	18501	198	0
3	POPC	40 × 40 × 25	5396	0	4	0	308565	0	152
	POPG		0	4864	4	0	287886	4864	152
	Mixture		2560	2560	4	0	294088	2560	152
4	POPG	40 × 40 × 25	0	4864	16	0	287886	4864	608
	Mixture		2560	2560	16	0	292088	2560	608

3.3 Initial structures

The initial structures of all systems were prepared with Packmol. Experimental values for the area per lipid A and the total bilayer thickness D_B were used to estimate the number of POPC and POPG lipids necessary to form membrane patches of the right sizes and heights.[47,48] The values used for the POPC/POPG membrane were interpolated as the mean value of the pure components as no data was available for this mixture. Table 3.2 lists the structural properties of the different lipid bilayers used for the preparation of the systems.

Table 3.2: Area per lipid and lipid bilayer thickness for POPC and POPG from experiments and for POPC/POPG from interpolation of the pure properties.

Lipid	Area per lipid A [nm^2]	Bilayer thickness D_B [nm]
POPC (301 K)[47]	0.593	3.9
POPC/POPG	0.626	3.8
POPG (301 K)[48]	0.660	3.7

A cross-section of a packed membrane patch with the planes and their heights with respect to the bilayer center are shown in Figure 3.1. The bilayer was prepared by packing each half of the lipids into a box with a height of 2.12 nm above and below the center of the box. The positions of two beads of the upper molecule half, including the head group, and two beads of the first lipid tail, were restricted to form the correct bilayer structure. In the upper layer the NC3 or GL0 (in POPC and POPG, respectively) and GL2 were restricted to be placed above a plane 1.42 nm above the center of the simulation box. Additionally the C1A and C4A beads were placed under a second plane 1.22 nm above the center. This results in a lipid monolayer. The opposing second lipid layer was build up the same way but inverted and in the lower box half.

Even with the mentioned restrictions, there was no real order in the lipid layers; also there is a small gap between the top and bottom layer. However, the gap vanished in the equilibration and the lipids equalized their distribution by themselves, which resulted in a stable lipid bilayers in the middle of the simulation box. The water beads were packed in boxes with

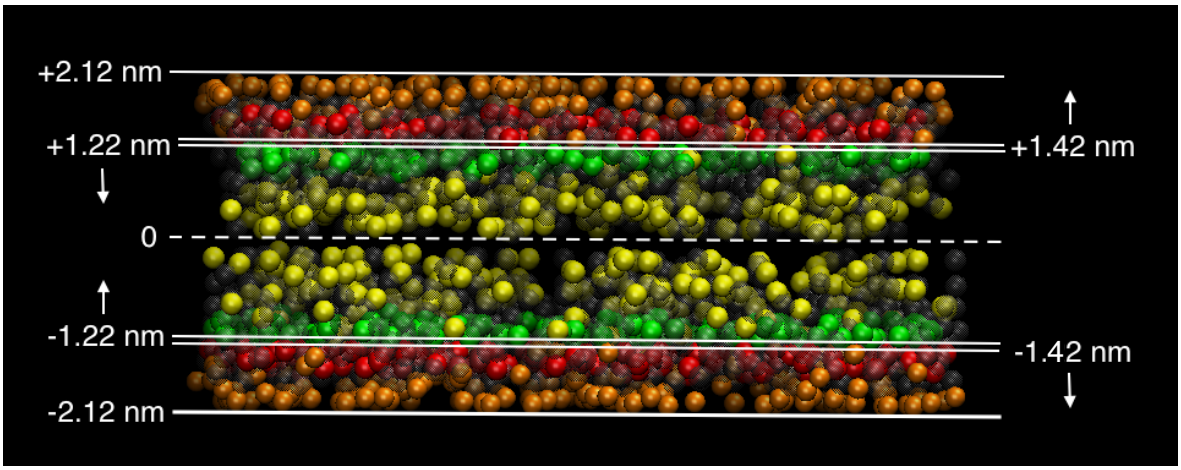

Figure 3.1: Cross section of an initial structure for a lipid bilayer generated with Packmol. The positions of the coloured beads (orange = NC3, red = GL0, green = C1A, yellow = C4A) are restricted, all other beads are displayed in transparent gray. The white lines show the positions of the planes used for the restrictions; the arrows indicate on which side of the planes the beads were placed, respectively.

a height of about 10 nm on both sides of the lipid bilayer. Counterion beads for the POPG molecules were then added by replacing randomly chosen water beads. This has been done with the `gmx genion` tool of the GROMACS software package.

The initial configurations of the systems that included nanoparticles were created using lipid bilayer and nanoparticle configurations from already finished NPT simulations. Therefor the corresponding output configuration of a membrane simulation was taken and the biggest part of the water molecules above the bilayer was removed, leaving only a thin layer of water (∼1nm) to preserve the hydrated state of the membrane. The nanoparticles, including their counterions, were placed above the bilayer. The final configurations of the NPT simulations from the model developing project have been used as input for the packing of the new systems. Then the empty space around the nanoparticles was packed with water. Figure 3.2 shows the structure of a packed system with a 10×10 nm membrane patch and one nanoparticle in which the gap between the already equilibrated lower part and the newly packed upper part, including the nanoparticle, is clearly visible. The advantage of this technique is that only a very short equilibration was necessary as the membrane had been equilibrated in an earlier simulation.

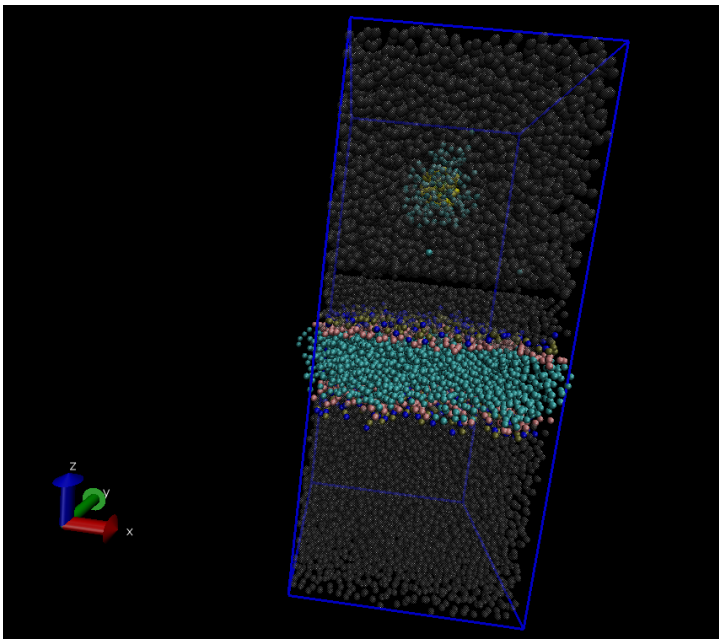

Figure 3.2: Initial configuration of a system containing one nanoparticle and a 10×10 nm lipid bilayer. The water beads are displayed in transparent gray to show the placement of the nanoparticle.

3.4 Equilibration

The initial configurations produced by Packmol were not suitable for being directly used as input for a NVT simulation. Therefore an energy minimization was performed after packing for all the systems, using a steepest-decent algorithm the energy minimizations converged after 20,000 to 100,000 steps.

The resulting structures were then equilibrated in a short NVT simulation of 25 ns at a temperature of 301 K using periodic boundary conditions in all directions. These general parameters were used in all equilibration and production runs. The integration of the equations of motion was performed using a leap-frog algorithm (GROMACS integrator `md`). Initial velocities assigned to the beads were randomly taken from a normal distribution for the corresponding temperature. To keep the membrane in the middle of the simulation box, the center-of-mass motion was removed in every step of this first equilibration. The following options were considered as advised with the MARTINI model:

- A time step of 25 fs was chosen for better energy conservation
- A cut-off of 1.2 nm for van-der-Waals interactions with a force-switch that, starting at 0.9 nm, smoothly brings the value of the potential to zero at the cutoff distance
- The particle-mesh Ewald (PME) method for calculation of electrostatic interactions

To increase the computational performance, a grid spacing of 0.2 nm and an interpolation order of 6 were used in the PME. This gives approximately the same accuracy as a grid spacing of 0.15 and an interpolation order of 4, which is a widely used cofiguration, but is more efficient in highly parallelized calculations.[49] In all equilibrations a Berendsen thermostat with a bath temperature of 301 K and a coupling constant of 5 ps was used due to its efficency and because a good description of the thermodynamic ensemble was not necessary at this point. Lipids, water molecules and nanoparticles each had separated groups for temperature-coupling. As the density of the systems had been slightly underestimated in the packing process, the two lipid layers seperated in some of the NVT equilibrations. However, they always reunited when the volume of the simulation box was freed in the NPT equilibrations.

Subsequently the resulting structures were used as input for a NPT simulation for another 250 ns (10^7 steps). The simulation parameters were almost identical to the ones in the NVT equilibration. As only difference isotropic pressure coupling was added while the volume of the simulation box was freed. A Berendsen barostat was used in the equilibration with a reference pressure of 1013 mbar, a coupling constant of 0.2 ps and a compressibility of 3×10^{-5} bar^{-1}.

After the NPT equilibration, the states of the equilibrated systems were investigated by use of the GROMACS `gmx energy` analysis tool. The temperature, the diagonal components of the pressure tensor, box lengths in x-,y- and z direction, average density as well as the energies for bonds, angles, Lennard-Jones and Coulomb interactions were calculated. Fluctuations of less than 2% were found for all these quantities. Only the pressure components showed bigger fluctuations, but around the desired medium value of 1013 mbar. With these results the equilibrations were considered successful for all systems.

3.5 Production

The production runs with a total simulation time of 2 µs (8×10^7 steps) were performed using the same simulation parameters as the NPT equilibrations. The only difference was a change in the coupling algorithms. Instead of the Berendsen barostat, which produces smaller fluctuations in systems that are not well-equilibrated, a Parrinello-Rahman barostat was used, which accurately preserves the ensemble. In this step, the coupling constant was increased to 1 ps. The Berendsen barostat was replaced by velocity-rescale temperature coupling, which has the advantages of the former but also produces the correct thermodynamic ensemble.

4 Results and discussion

4.1 Membrane simulations without nanoparticles

Three lipid bilayer patches, build up from pure POPC, pure POPG and a mixture of POPC and POPG, in a molar ratio of 1:1, have been simulated. The results were used to compare the bilayer properties in the simulations with experimental data and as a reference for the unperturbed membranes in the absence of nanoparticles. Before the calculation of other properties it was ensured that the surface tension γ of the bilayer was zero in the simulations. It was calculated from the diagonal elements of the pressure tensor $\mathbf{P}$ as shown in equation 4.1.

$$\gamma = \mathbf{P}_{zz} - \frac{1}{2}\left(\mathbf{P}_{xx} + \mathbf{P}_{yy}\right) = \mathbf{P}_{zz} - \bar{\mathbf{P}}_{xy} \tag{4.1}$$

If there is significant deviation in the average pressure in the xy-plane $\bar{\mathbf{P}}_{xy}$ and the pressure in z-direction $\mathbf{P}_{zz}$, the membrane cannot be considered tensionless. In experiments the surface tension is normally zero as the membranes are much bigger than in MD simulation. Therefore it is important to ensure that there is no surface tension in the membrane simulations when comparing the properties with experiments. The diagonal elements of $\mathbf{P}$ have been calculated with the `gmx energy` analysis tool. The calculated surface tensions for the three bilayers can be found in table 4.1 together with other relevant properties (see below).

Table 4.1: Membrane properties for the three membranes from the simulations without nanoparticles.

Lipid	$\bar{\mathbf{P}}_{xy}$ [mbar]	$\mathbf{P}_{zz}$ [mbar]	γ [mbar]	A [nm^2]	D_B [nm]	$S_Z(1)$	$S_Z(2)$
POPC	1033±8	1029±7	4±11	0.653	3.77	0.661	0.656
POPC/POPG	1034±10	1020±6	14±12	0.646	3.90	0.670	0.668
POPG	1034±9	1028±6	6±11	0.656	3.85	0.586	0.581

It can be seen that all three bilayers are tensionless when the errors are taken into consideration. Also the very small uncertainties of the elements of the pressure tensor show that the pressure in the simulations is well-equilibrated. The next properties, that were calculated, were the area per lipid A and the total bilayer thickness D_B. They are also listed in table 4.1. The values from the simulation were compared to the experimental values from table 3.2. Although these values have been used for the preparation of the system, the properties of the membranes have changed to their actual values in the MARTINI model during the equilibrations and subsequent simulations. However, there were only small deviations from the experimental values. The bilayer thickness showed maximum deviations of 5% for all membranes, while the maximum deviation for the area per lipid was 10%. Surprisingly the area per lipid of POPC and POPG was very similar in the simulation while the experimental data show a substantial difference. More interestingly, the values of the mixed bilayer did not lie in between the values of the pure ones. Instead, the average area per lipid was smaller, while the membrane thickness was higher than suggested by the interpolation. This shows that the mixing of the two lipids is actually preferred in these simulations, which is reasonable as the negative head groups of the POPG lipids repel each other. To reduce the total electrostatic energy, a maximization of the distance between these molecules takes place, resulting in a stable mixture of the two lipids in the bilayer.

The order parameter S_z for the lipids in the bilayers were investigated. It can be calculated from the angle ϑ_z, which is the angle between vector connecting the lipid head group with the end of one of its tails and the normal of the membrane plane, as shown in equation 4.2. It has values from -0.5 to 1 with 1 representing perfect alignment along bilayer normal, 0 no order at all and -0.5 a perfect alignment along the plane of the lipid bilayer.

$$S_z = \frac{3}{2}\left\langle \cos^2(\vartheta_z)\right\rangle - \frac{1}{2} \tag{4.2}$$

As the plane of the membrane in the simulations is, in good approximation, the xy-plane, the elementary vector in z-direction was used instead of the normal of the plane. The vector of the lipid orientation has been calculated as

difference of the positions of the PO4 and the C3A or C3B bead, respectively, using the `gmx order` analysis tool. The outermost beads NC3 and C4A/C4B were not used due to their high mobility that would artificially reduce the order parameter. This resulted in two order parameters $S_Z(1)$ and $S_Z(2)$ for each lipid composition, which are also listed in table 4.1. The monounsaturated lipids considered in the simulations should always be in the fluid state, as their transition temperatures are below 0°C. This state is characterized by order parameters between 0.6 and 0.8, while a gel phase at lower temperatures is characterized by values bigger than 0.8 for the order parameters. The order parameters calculated from the simulations are all within this range and prove that the membranes are in a fluid state in all three simulations (see table 4.1).

For a detailed look at the membrane structure the number density profiles of the three membranes as function of the z-coordinate were calculated with the `gmx density` analysis tool. Figure 4.1 shows the resulting density profile of the POPC bilayer.

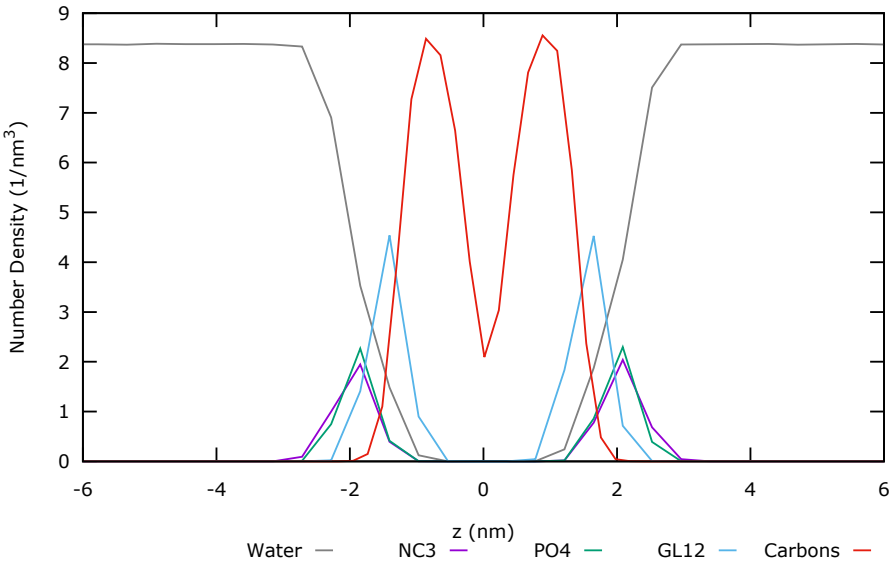

Figure 4.1: Number density profile of the POPC bilayer in z-direction. As common for these density profiles, the last carbon beads in the lipid tails have been left out, to make the border between the two layers visible.

The bilayer shows a high symmetry in both layers in the height and the positioning of all peaks, as expected. Also the distances between the maxima is reasonable when compared to the average bond lengths. The peaks of the two lipid head group beads completely overlap, even though they actually are surrounded by water. This is caused by the zwitterionic nature of the head groups in the POPC. By flattening out on the membrane surface, the ionic beads in the head groups are able to form ion pairs with oppositely charged beads of the neighboring head groups. The number density profiles of the other lipids showed the same overall behavior except for the overlap of the head group beads. They are shown in subsection 4.2.2 when the influence of the nanoparticles on the density profiles of the membranes is discussed.

Overall the lipid bilayers in the simulations show the expected behavior and are in good agreement with experimental data. Therefore they can be considered good membrane models for the investigations in this work.

4.2 Membrane simulations with nanoparticles

4.2.1 Nanoparticle attachment

The first stage of simulations contained one anionic or cationic nanoparticle and 10×10 nm membrane patches of POPC, POPG or a mixture of these two lipids, resulting in a total of six different combinations. The nanoparticles were placed approximately 6 nm away from the bilayer to study the general behavior of the systems without any biasing of the simulations. Also, the affinities of the different combinations of lipids and nanoparticles were investigated. Furthermore the z-distance between the nanoparticle center of mass and the middle of the lipid bilayer was calculated as function of the simulation time. The results of this analysis for the six systems are presented and shortly discussed in the following.

POPC + positive nanoparticle: Figure 4.2 shows that the nanoparticle attached to the neutral POPC membrane quickly and stayed there for the majority of the simulation time while still being able to detach. The closest distance between the two centers of the nanoparticle and the bilayer is about 4 nm, which corresponds to the lipid head groups being in contact with the charged carbon beads of the alkyltholate ligands.

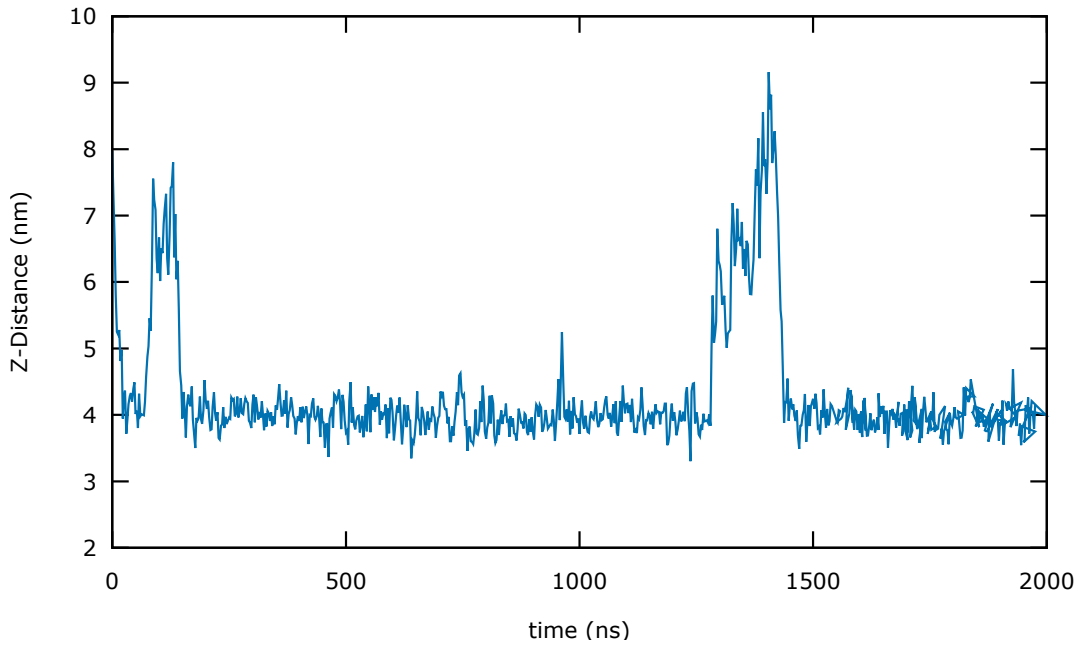

Figure 4.2: z-distance between the centers of the cationic nanoparticle and the POPC bilayer during the simulation.

POPC + negative nanoparticle: The negative nanoparticle shows similar behavior, as can be seen in figure 4.3. Though it is not able to detach itself from the bilayer the contact distance indicates that the binding type and thus the binding strength is also comparable to the positive nanoparticle. This behavior was expected, as the only difference between the two nanoparticles is the sign of their charges.

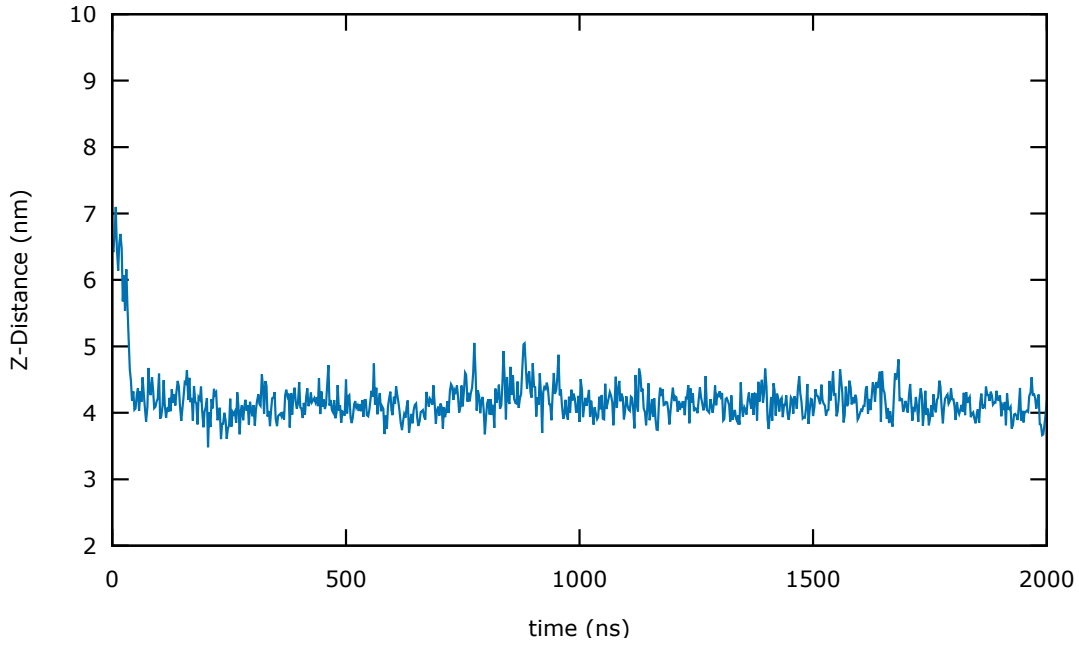

Figure 4.3: z-distance between the centers of the anionic nanoparticle and the POPC bilayer during the simulation.

POPC/POPG + positive nanoparticle: On the mixed bilayer, that has a negatively charged surface, the cationic nanoparticle bound to the bilayer after a a short time of free diffusion (see figure 4.4). There is no detachment at all. After the first contact at a distance of 3.3 nm the nanoparticles gets closer to the membrane in the next 500 ns, reaching its final, stronger state of attachment at a distance of 2.8 nm after 800 ns.

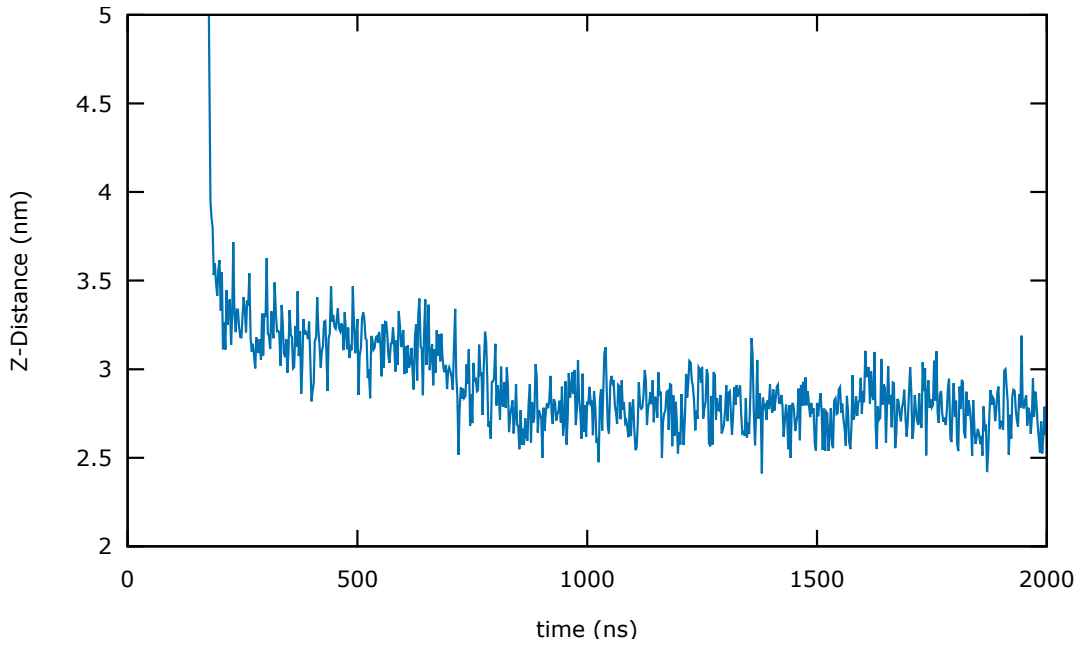

Figure 4.4: z-distance between the centers of the cationic nanoparticle and the POPC/POPG bilayer during the simulation.

POPC/POPG + negative nanoparticle: The behavior of the negatively charged nanoparticle on the mixed bilayer is illustrated in figure 4.5. As one can see the nanoparticle needs a long time to get in contact with the bilayer and even then the attachment is not permanent.

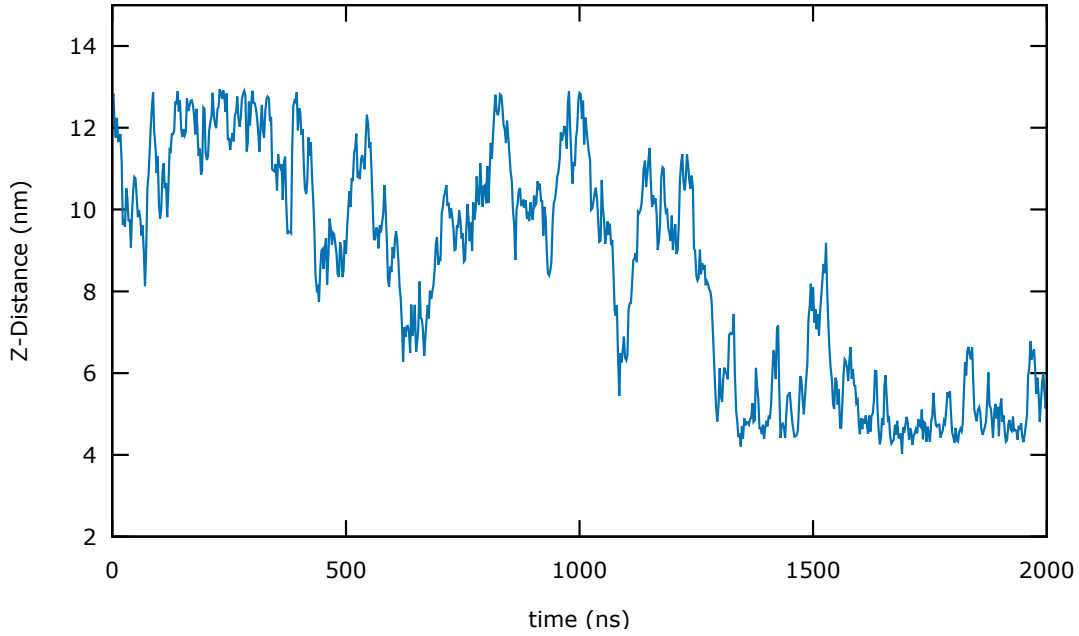

Figure 4.5: z-distance between the centers of the anionic nanoparticle and the POPC/POPG bilayer during the simulation.

POPG + positive nanoparticle: The cationic nanoparticle attaches immediately to the negative POPG bilayer (see figure 4.6). Again, there are two binding states at distances of 3.1 and 2.6 nm.

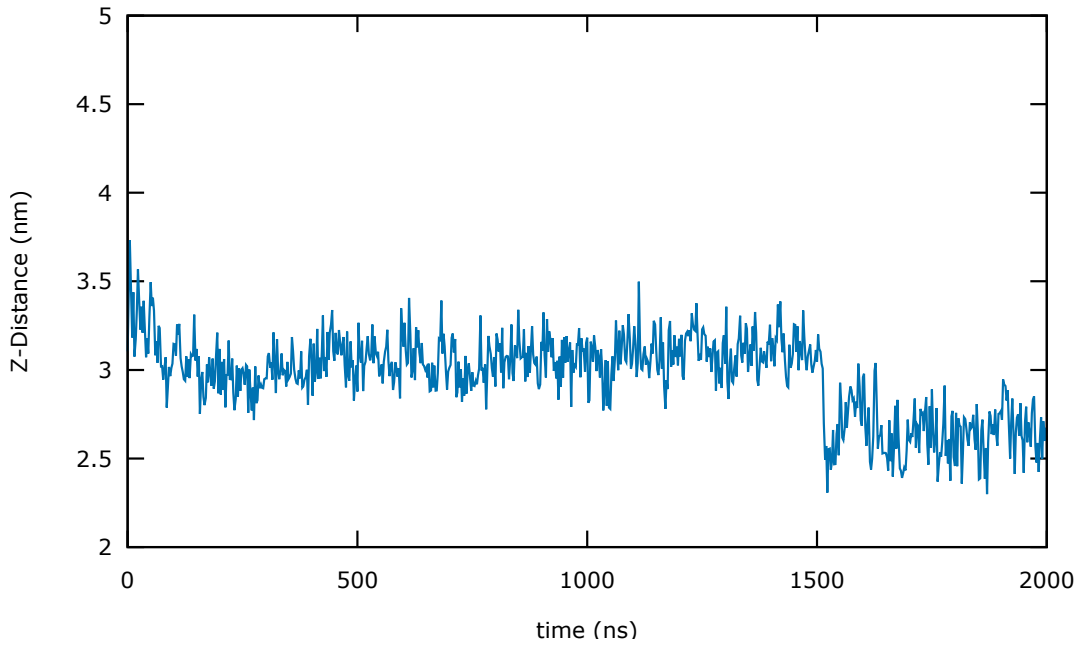

Figure 4.6: z-distance between the centers of the cationic nanoparticle and the POPG bilayer during the simulation.

POPG + negative nanoparticle: In figure 4.7 the movements of the anionic nanoparticle with respect to the center of the POPG membrane is shown. Due to the identical charges, the nanoparticle cannot attach to the membrane as it is repelled, as soon as the lipid head groups and the alkythiolate ligands come close to each other.

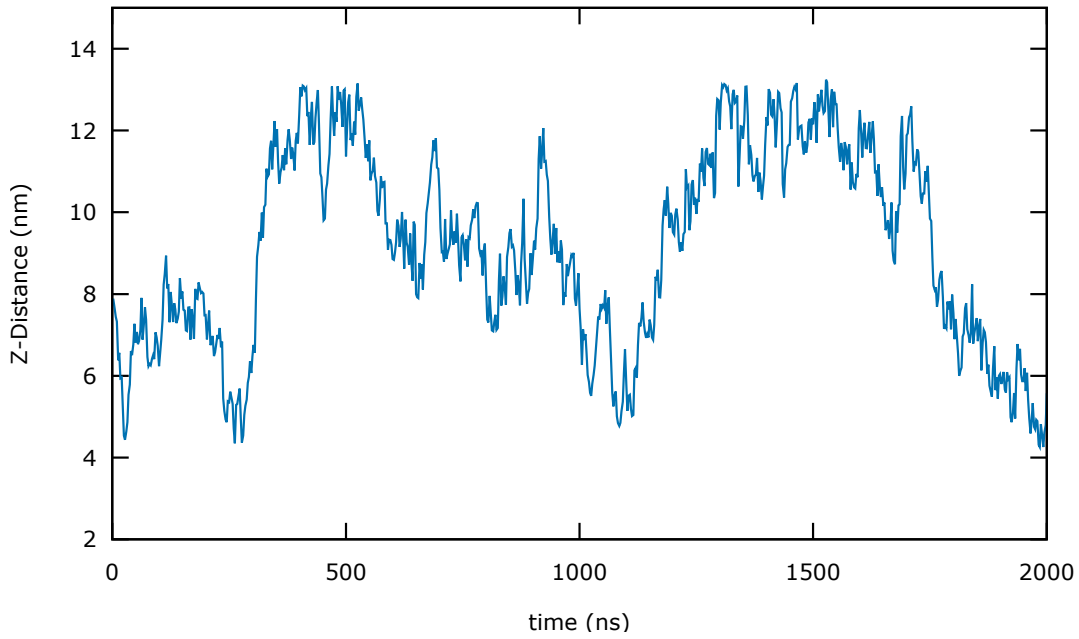

Figure 4.7: z-distance between the centers of the anionic nanoparticle and the POPG bilayer during the simulation.

Table 4.2 summarizes the affinities of the nanoparticles to the different lipid bilayers. Thereby some conclusions can be drawn: As expected, the nanoparticles with opposite charges behave identical in the POPC system, in which the membrane surface has no overall charge. Without Coulomb attraction between the nanoparticles and the membrane surface, there is only a weak attachment. This is in agreement with the experiments of Montis *et al.* that showed an

Table 4.2: Attachment behavior of the investigated systems with minimum distances between the centers of the lipid bilayer and the nanoparticle. If two binding states were observed, the distance of the weaker one is given in parentheses.

	NP positive	**NP negative**
POPC	weak attachment detachment possible 4.0 nm	weak attachment detachment possible 4.0 nm
POPC+ POPG	strong attachment no detachment 2.7 nm (3.2 nm)	very weak attachment fast detachment 4.5 nm
POPG	strong attachment no detachment 2.6 nm (3.1 nm)	no attachment 4.5 nm

attachment of the cationic nanoparticles to POPC and POPC/POPG bilayers.[17] In the simulations with the negatively charged POPC/POPG and POPG membranes the anionic nanoparticles were repelled, while the cationic nanoparticles attached very quickly. The latter ones got in much closer contact than on the neutral bilayer after being in a weaker, metastable state of attachment. This behavior can be considered similar to the first two steps of the three-staged insertion process observed in coarse-grained simulations by Simonelli *et al.* (see section 1).[21] The stronger nanoparticle attachment was irreversible on the time scale of the simulations. It remains unclear if the stronger binding state is generally accessible and/or stable for the nanoparticles on the POPC bilayer. However, the electrostatic attraction seems to be the driving force for a quick and irreversible binding of the nanoparticles to the bilayer. This is in agreement with the simulation results of Lin *et al.* as well as the observation of a stronger binding of cationic nanoparticles to negatively charged membranes.[25] Their results do not show a metastable intermediate state of attachment, maybe because the nanoparticles are forced to move to the bilayer. However, their free energy calculations also only show one global minimum in contact with the bilayer for the nanoparticles.

The irreversibility of the nanoparticle attachment on the POPC/POPG and POPG membranes is most probably an entropic effect. As the nanoparticle gets in contact with the membrane, the chloride counterions of the nanoparticle form ion pairs with the sodium couterions of the POPG. These ion pairs then move away from the bilayer into solution, making the attachment irreversible. This also explains why this irreversibility is not observed in the simulations with a zwitterionic membrane and may be the reason that keeps the nanoparticles from reaching the stronger state of attachment during the time scales of the simulations.

Overall the nanoparticles showed a reasonable behavior, especially the desired attachment to the lipid bilayers that is crucial for the further investigations in this work. However, the negative nanoparticles were not used in the following simulations, as they showed no binding to the negative bilayers and the same behavior as their positive counterparts on the neutral membrane.

4.2.2 Static properties

In this subsection 4.2.2 the results showing the influence of the nanoparticles on the structure of the membranes are presented and discussed. Thereby the main focus was on the changes of the area, thickness and density profile of the lipid bilayers, the local order of the lipids and the distribution of multiple nanoparticles on the bilayer surface. The results discussed in this first paragraph were obtained from the simulations of the third stage containing 4 cationic nanoparticles placed on one side of a 40×40 nm membrane patch. Again, the nanoparticles attached themselves to the bilayers without any biasing. However, the initial distance between the nanoparticles and the membrane had been reduced, so that the nanoparticles bound to the membrane within the equilibration. Also in the attachment strengths, the bigger systems showed the same behavior as their smaller analogs.

There was no significant change, neither in the area per lipid nor in the thickness of the bilayer in any of the three simulated systems. All membranes were confirmed to be tensionless. This was also confirmed by the later simulations of the fourth stage, containing more nanoparticles. However, a significant influence of the nanoparticles on the density

profile of the lipid bilayers was observed. Figure 4.8 shows the number density profiles for the POPC, the POPC/POPG and the POPG bilayer with and without attachment of four positive nanoparticles. Without nanoparticles the density profiles of the three membranes look very similar with only a small difference in the peaks of the head group beads in POPG bilayer, as discussed in 4.1. In the presence of the nanoparticles the perturbation of the density profiles increases with the negative surface charge of the bilayer. While there is almost no noticeable change in the POPC bilayer due to the weak attachment of the nanoparticle, the perturbation becomes obvious in the other systems. Interestingly, there is a much stronger perturbation in POPG bilayer than in the mixed one, even if the contact distance of the nanoparticles are identical. In the mixed membrane only the layer facing the nanoparticle is mildly perturbed. On the other hand, also the structure of the lipid tails from the opposing layer is influenced significantly in the POPG bilayer. This shows that electrostatic interactions play a major role in the strength of the attachment and not only in the attachment process.

In the simulations of the fourth stage the number of positively charged nanoparticles on the bilayers was increased to 16 using a POPC/POPG and a POPG membrane. This was done to increase the overall effect of the nanoparticles and the sample size for the following analysis. This favored the investigations of the interactions between the nanoparticles on the membrane surface, too. The pure POPC system was abandoned at this stage due to the very weak influence of the nanoparticles on the bilayer seen in the density profile. Unfortunately three nanoparticles attached to the opposite site of the membrane in the POPG simulation, crossing the periodic boundary in z-direstion. The eventual implications of this on the results obtained from these simulations will be discussed in the following. The results discussed in the following were obtained from the simulations with 16 nanoparticles.

Firstly, the local order parameters of the POPC and POPG lipids in the mixed bilayer and the POPG bilayer were calculated using the custom analysis tool `localorder`. This tool calculates the order parameters based on a provided selection. The complete program code can be found in the appendix. In this case the same two bead combinations as described in subsection 4.1 were used for the calculations. In this case individual order parameters were calculated for lipids in the top and bottom layer of the membrane. These lipid were again split in two groups each: One, the center of mass of which was inside a cylinder with a radius of 3 nm around the nanoparticle and another one, in which the lipid centers were outside of mentioned cylinders. This resulted in a total of 16 parameters. They results for the mixed bilayer are listed in table 4.3. The results for the POPG lipids in the pure POPG bilayer are similar to the ones from the POPC/POPG bilayer and therefore not shown separately, because of the corruption of the data due to the nanoparticles that attached to the lower lipid layer.

Table 4.3: Local order parameters for the different lipids, tails (1 and 2), layer (top and bottom) and distance from the nanoparticle in the POPC/POPG bilayer.

	Close to NP		**Far from NP**	
	top	bottom	top	bottom
POPC-1	0.647 ± 0.018	0.702 ± 0.010	0.683 ± 0.014	0.687 ± 0.014
POPC-2	0.612± 0.018	0.671 ± 0.010	0.657 ± 0.014	0.662 ± 0.013
POPG-1	0.571 ± 0.017	0.703 ± 0.011	0.686 ± 0.014	0.692 ± 0.014
POPG-2	0.584 ± 0.016	0.676 ± 0.011	0.661 ± 0.014	0.669 ± 0.013

In all groups there is no difference in the order parameters of the two lipid tails when considering the uncertainties. The fact that the values are a little smaller for the second lipid tail is caused by the lipid geometry as the first tail is connected to the head group in a straight line of atoms, while the second tail is connected as a branch. Also the order parameters in the top and the bottom layer are identical when the lipids have no direct contact with one of the nanoparticles. A significant change in the order parameters can only be observed close to the nanoparticles. In the top layer facing the nanoparticles the order parameters drop by about 7% for POPC and 15% for POPG compared to the regions away from

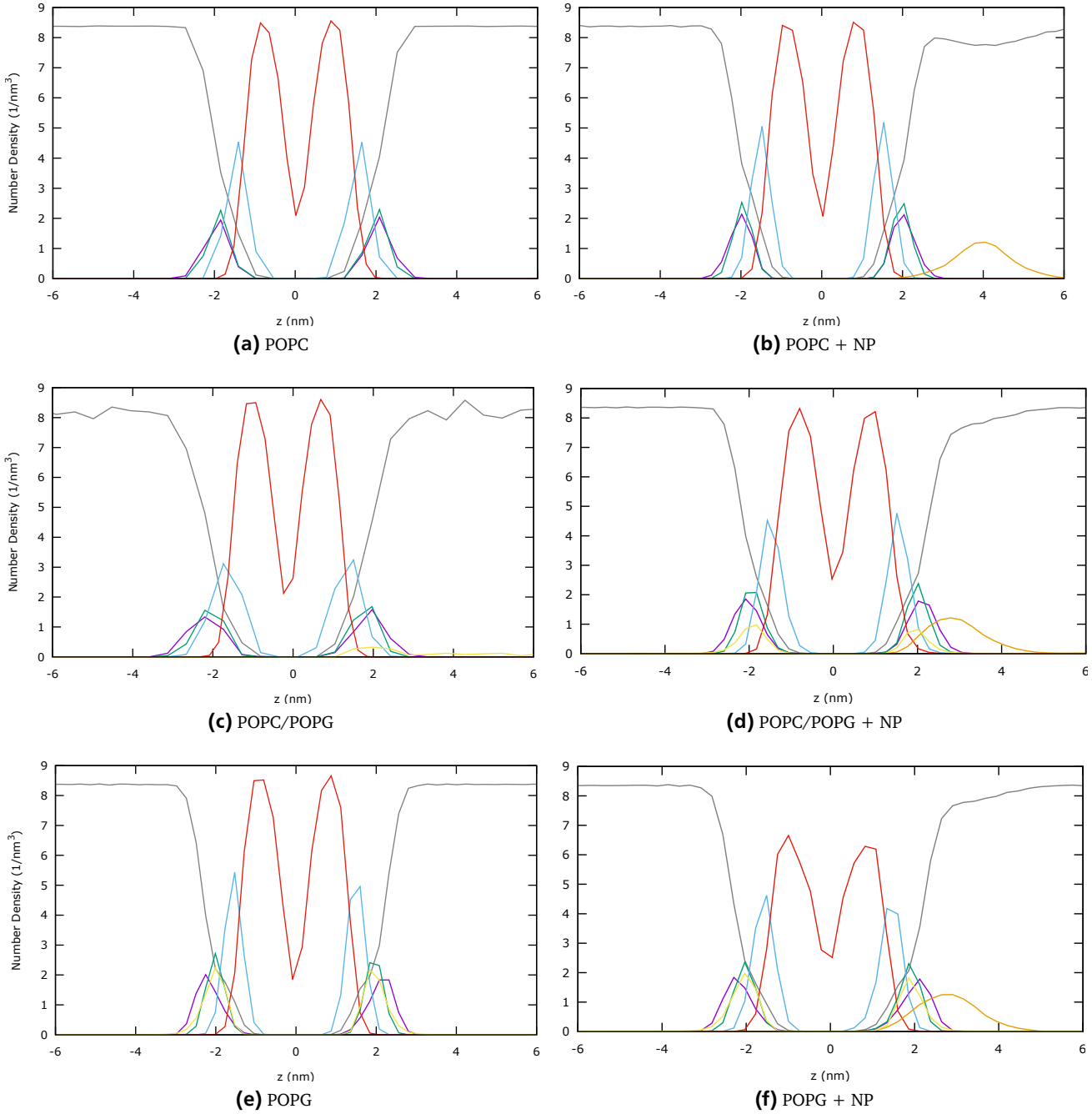

(a) POPC **(b)** POPC + NP

(c) POPC/POPG **(d)** POPC/POPG + NP

(e) POPG **(f)** POPG + NP

Figure 4.8: Number density profiles of the three bilayers without (left) and with 4 cationic nanoparticles (right). Color scheme: red = carbon tail beads (C1A, D2A, C3A and C1B-C3B), light blue = connecting beads (GL1, GL2), yellow = sodium (NA+), green = phosphate bead (PO4), purple = outermost head group bead (NC3 and/or GL0), ochre = nanoparticle core and ligands, gray = water beads (W).

the nanoparticles. In the bottom layer no significant influence of the nanoparticle was observed. This shows that the nanoparticle has a strong influence on its close surrounding on the monolayer that faces it, but does not change the membrane structure globally. Interesting is the fact that the order of the POPG lipids is perturbed much more than the order of the POPC lipids. The local order parameters calculated for the POPG membrane, in which the nanoparticles on the bottom side of the bilayer were not considered, showed no significant deviation from the POPG lipids in the mixed bilayer.

The reason for the difference in the local order parameters of the POPC and POPG lipids close to the nanoparticles is a change in the local composition of the bilayer in the neighborhood of the nanoparticles. In other words there is preference

of POPG over POPC in their direct surrounding. To illustrate this, two snapshots from the simulation of the mixed bilayer in top view are shown in figure 4.9. As one can see, there is a high concentration of the yellow POPG molecules visible in the left periodic image where the nanoparticles are positioned in the right periodic image. The nanoparticles change the local composition of the membrane in the lipid layer facing them. This effect is not visible in the opposing lipid layer, as the lipid tails that may interact with the nanoparticles are identical for POPC and POPG. In the simulation used for this investigation there was no total demixing of the lipids in the membrane.

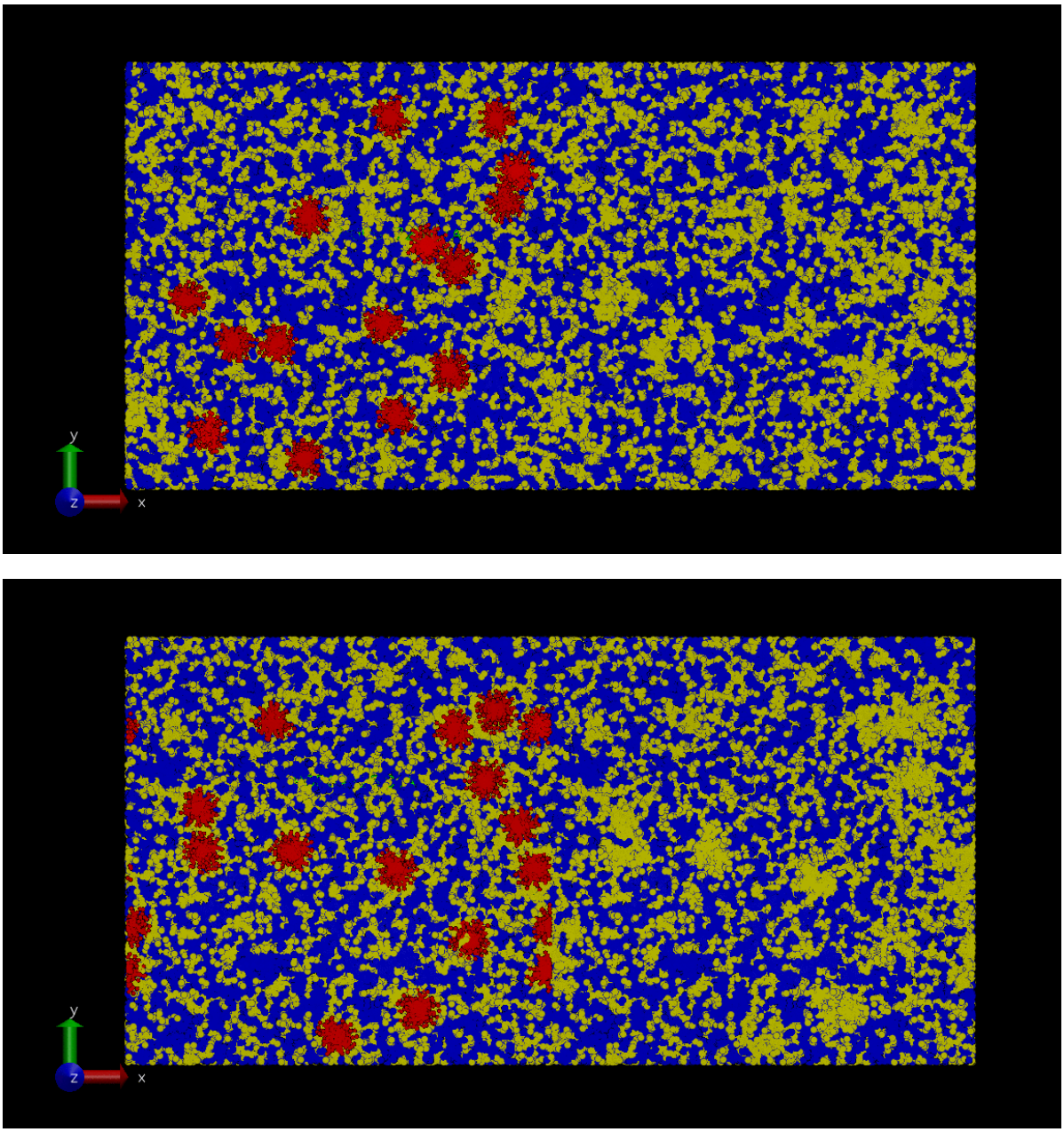

Figure 4.9: Two snapshots from the simulation of the POPC/POPG bilayer with visible nanoparticles in the left and invisible nanoparticles in the right periodic image. Color scheme: POPC = blue, POPG = yellow, nanoparticles = red.

For a more quantitative investigation of this phenomenon the lateral radial distribution functions of the POPC and POPG head group beads (NC3 or GL0, respectively) with respect to the centers of mass of the nanoparticles have been calculated using the `gmx rdf` analysis tool. The resulting graph is shown in figure 4.10. It confirms the higher affinity of POPG to the nanoparticle, compared to POPC. It is also obvious that the majority of the lipid head groups is pushed to the sides of the nanoparticle, so that the sulfur beads and the gold core get in contact with the carbon beads of the underlying lipids. The formation of similar structures has been reported by Heikkilä *et al.* in atomistic simulations of cationic alkylthiolate coated gold nanoparticles on POPC/POPS membranes.[22] This shows that the MARTINI model is able to reproduce the

structures from atomistic simulations. Additionally, the influence of the nanoparticle on the local composition of the membrane is bigger than expected from the simulation snapshots. The distance in which the concentrations of the lipids reach their equilibrium values is 6 nm. This is much more than the radius of the nanoparticle, which is 2 nm including the ligands, plus the cut-off of 1.2 nm used in the MARTINI model. A possible explanation of the long radius of influence is that the relaxation of the composition is a little slower than the lateral movements of the nanoparticles. Also the overestimation of the electrostatic interactions in the MARTINI model could be responsible for this. However, this effect will most probably depend heavily on the nanoparticle size, concentration and surface charge density as well as the lipids in the bilayer.

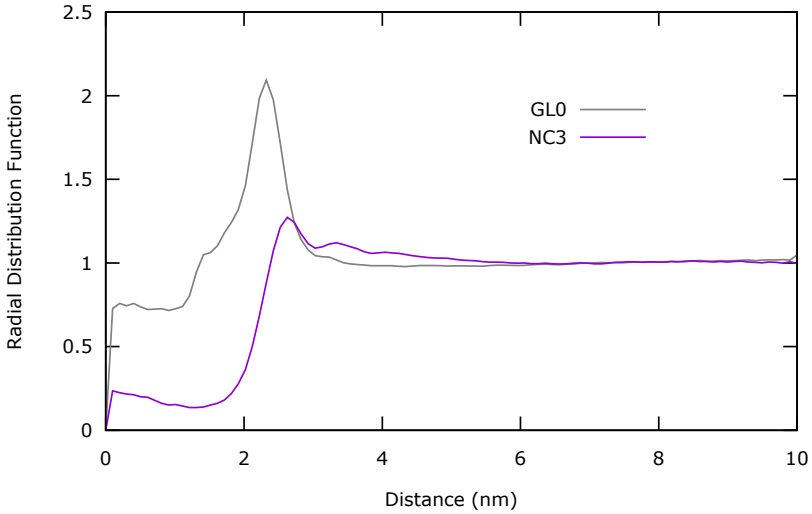

Figure 4.10: Lateral radial distribution of the POPC (gray) and POPG (purple) headgroups in the upper lipid layer around the center of the nanoparticles.

Experiments show the formation of domains in POPC/POPG vesicles in the presence of cationic gold nanoparticles.[17] However, these domains are way larger than the size of the simulation boxes used in this work. It also remains unclear if these domains actually differ only in composition or show structural deviances as well. It therefore is arguable if the reason for this domain formation is the effect observed in the simulations, just on a larger scale, or a completely different one.

The mentioned experiments also suggest a formation of nanoparticle clusters on the membrane surface.[17] While there is no formation of stable nanoparticle cluster in the simulations, there is a weak form of self-assembly. As can be seen in figure 4.9, the nanoparticles are not distributed equally over the whole POPC/POPG membrane surface, although they are lightly repelling each other. This can be seen in the lateral radial distribution of the nanoparticles on the different membranes, which is shown in figure 4.11. It clearly shows that other nanoparticles are preferred at distances of 5.0 and 7.8 nm on the mixed bilayer. As mentioned before, this cannot be explained by a direct attraction between the nanoparticles. Instead a reasonable explanation would be that the changes of the membrane composition caused by the nanoparticles are the reasons for the relatively close contact of the nanoparticles on the membrane. By increasing the POPG concentrations in their surroundings the nanoparticles create POPG patches that are more attractive for other nanoparticles. Also POPG lipids can be directly exchanged between neighboring nanoparticles when they are in close contact. This hypothesis is supported by the distribution of the nanoparticles on the POPG bilayer, which shows only one peak at a distance of about 6 nm, which is also smaller. Overall the nanoparticles are almost evenly distributed on the POPG membrane. The observed arrangements of nanoparticles, especially in the simulations of the POPC/POPG bilayer, could be the clustering observed in the experiments. However, to verify this detailed information about the concentration and the distribution of nanoparticles on the vesicles in the experiments are needed.

Despite the strong effects of the nanoparticles on the membranes, no signs of a disruption or penetration of the membranes were observed in any of the simulations. This is reasonable as there are no reports of unbiased simulations using similar models that are able to show these effects. The lipid bilayers in the MARTINI model are quite stable and also their stiffness is rather high due to the small system size. In comparison with the scales of the simulations, the experimental membrane dimensions of the membranes are infinite, which makes it possible to wrap nanoparticles. This effect is impossible to observe in simulations with the time and length scales used in this work. After all, the reproduction

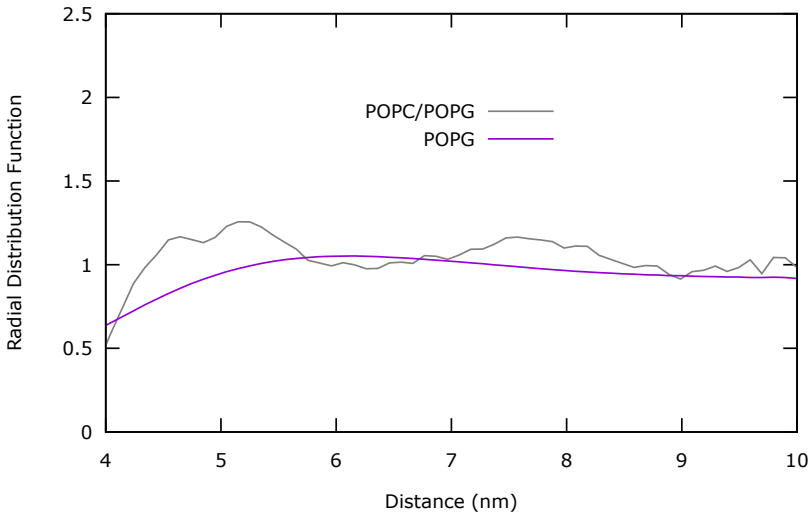

Figure 4.11: Lateral radial distribution of the nanoparticles on the POPC/POPG (gray) and the POPG bilayer (purple).

of these experimental observations is not of importance in this work, as the focus is on the interactions of nanoparticles with stable membrane rather than their disruption or penetration.

4.2.3 Dynamic properties

For the investigation of the dynamic properties of the bilayer, only the simulations containing 16 positively charged nanoparticles have been used. The main reason for this was the increased sample size, as the convergence has been shown to be the major obstacle in the analysis of the dynamic effects. Reference values for the unperturbed membranes were calculated from the simulations of the first stage.

The main focus of the investigations was on the influence of the nanoparticles on the lateral diffusion of the lipids in the POPC/POPG and POPG bilayer. The lateral global diffusion coefficients D were calculated for each type of lipid in the two simulations with the `gmx msd` analysis tool which uses a linear fitting of the mean square displacement as shown in equation 4.3.

$$D = \lim_{t\to\infty} \frac{1}{6t} \langle |\vec{r}(t) - \vec{r}_0|^2 \rangle \tag{4.3}$$

They were compared to the ones from the membrane simulation without nanoparticles. The results are shown in table 4.4 together with the lateral diffusion coefficients of the cationic nanoparticles on the membranes.

Table 4.4: Lateral diffusion coefficients in the POPG and POPC/POPG bilayer in 10^{-5} cm^2s^{-1} in the absence and presence of nanoparticles.

	without NP	**with 16 NPs**	**NP**
pure POPG	0.0704 ± 0.0015	0.0504 ± 0.0109	0.0122 ± 0.0053
POPC/POPG (POPG)	0.0582 ± 0.0011	0.0564 ± 0.0057	0.0260 ± 0.0074
POPC/POPG (POPC)	0.0593 ± 0.0050	0.0567 ± 0.0030	

As one can see the lateral diffusion is significantly reduced in the POPG bilayer while this is not the case for both lipid types in the POPC/POPG bilayer. Also the nanoparticles seem to move faster along the mixed bilayer, but unfortunately

the error bars are too big to be sure about it. However, the lateral diffusion of the nanoparticles is slower than the one of the lipids but still within the same order of magnitude. Diffusion coefficients for the lipids in giant unilamellar vesicles with and without the presence of gold nanoparticles were measured by Montis *et al.*. The free lipids had a diffusion rate of 0.008×10^{-5} cm^2s^{-1}, while it was reduced to 0.002×10^{-5} cm^2s^{-1} for the lipids affected by the nanoparticle. In the experiments, the latter value is also considered to be the diffusion rate of the gold nanoparticles on the membrane surface as it could not be measured individually. Due to the accelerated dynamics in the MARTINI model, the experimental diffusion coefficients cannot be compared directly. It is also obvious that the diffusion rates from the simulations are much higher than the ones from the experiments, even after applying the standard conversion recommended for the MARTINI model, which is a multiplication by a factor of 4.[30] However, the relative difference in the diffusion rates of the lipids and the nanoparticles in the simulation is in agreement with the experiments.

To get detailed insight in the influence of the nanoparticles on the lateral diffusion of the lipids, several attempts have been made. Most of them, unfortunately, were not able to provide converged or significant results due to the limited sample sizes, the short simulation times or the limited amount of data that could be stored and analyzed. These approaches are discussed at the end of this subsection. Before, the results provided by calculation of the molecular diffusion coefficients are presented and discussed. The distribution of the molecular diffusion coefficients were rather broad due to the limited simulation time and small sample size of about 5000 lipids. Figure 4.12 shows the results for the POPG bilayer.

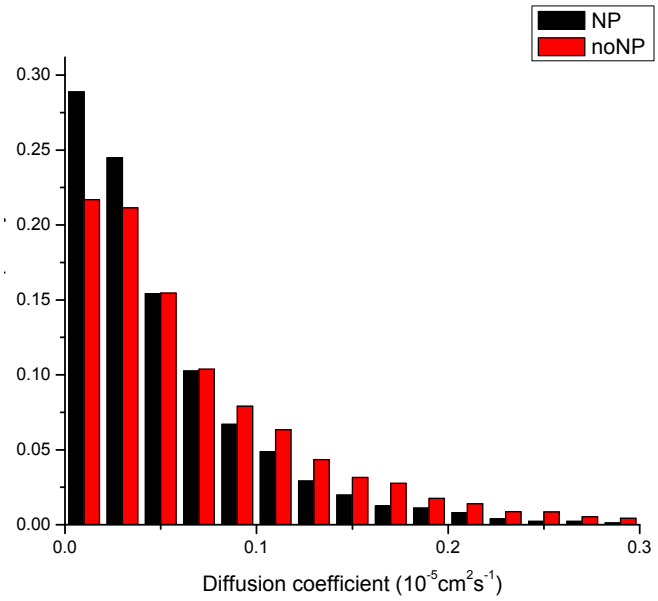

Figure 4.12: Distribution of the molecular diffusion coefficients in the POPG bilayer with (black columns) and without nanoparticles (red columns).

There is a noticeable shift of the distribution to the low diffusion region when nanoparticles are present. Especially the first two columns, which represent the same diffusion coefficients as the nanoparticles on the bilayer, grew considerably, while the regions of high diffusion lost the highest percentage. The same effect can be seen in the POPC/POPG bilayer, even if it is not as strong as in the POPG membrane. Figure 4.13 shows the individual distributions for the POPC and POPG lipids in the mixed bilayer.

The reason for this reduction of the lateral diffusion was discovered, when single lipid molecules were observed during the simulation. When the lipids are not close to a nanoparticle they diffuse freely in the bilayer. If they then encounter a nanoparticle, there is a probability that they attach to it. The nanoparticle and the lipid then diffuse together, of course with the lower diffusion rate of the nanoparticle, for some time before they part and the lipid diffuses freely again. This behavior was observed for all randomly chosen lipids and nanoparticles in the two simulations. Snapshots from the simulation of the POPC/POPG bilayer, that illustrate this, can be found in the appendix. This behavior is most probably what has been reported as formation of raft-like domains in the presence of gold nanoparticles in lipid bilayers by Montis *et al.*[17] and is to date the first confirmation of their interpretation. Several attempts were made to quantitatively prove this correlation, but have not yet been successful. Nonetheless they are presented and discussed in brief.

Velocity autocorrelation functions (ACFs) were calculated for the POPC and POPG lipids in the simulations for comparison with experimental data from Montis *et al.*.[17] This ACF is connected to the diffusion coefficient via the Green-Kubo integral

shown in equation 4.4. The idea was to fit the ACFs with two relaxation constants to show that there are two different fractions of free and attached lipids with different diffusion coefficients. Unfortunately, the small sample number of lipids made it impossible to reach convergence with the amount of data that could be stored and analyzed because the decorrelation times in the simulation were very short (~1 ns).

$$D = \frac{1}{3}\int_0^\infty dt\langle\vec{v}(t)\vec{v}(0)\rangle \tag{4.4}$$

Another attempt was made to correlate the reduction of the diffusion rates of the lipids with the time fraction they spend close to the nanoparticle in the simulation. Therefor another costumized analysis tool named fractions was written. Its program code can be found in the appendix. This simple tool counts the number of frames in the simulations, that each lipid molecule spends within a cylindrical element with a height of 4 nm and a radius of 2 nm around a nanoparticle. At the end it divides this number by the total number of frames and thus provides the time fraction spent attached to a nanoparticle in the simulation for each molecule. If this data is combined with the diffusion coefficients of each lipid during the same time, it would be possible to show the correlation between the time spent of the nanoparticle and the reduction of the diffusion rate. However, this attempt was not able to provide meaningful results either. The problem were the different requirements for good results in the two parts. To get well-converged values for the molecular diffusion, a very long trajectory has to be considered. If this is done, the fraction of lipids that spend enough time with the nanoparticle to show a significant difference in their diffusion rate gets smaller. To get a high percentage of lipids that spend a high percentage of the simulation time attached to nanoparticles, only a small part of the trajectory can be chosen as in this time some lipids spend almost all their time with the nanoparticles without leaving it. Besides the fact that the number of lipids, that are influenced by nanoparticles, is very small the diffusion coefficients do not converge in this short amount of time. In other words, the main problem is either the slow convergence of the diffusion coefficients or the inability of the fitting of the mean-square displacement to show the different diffusion rates of a single molecule during the simulation.

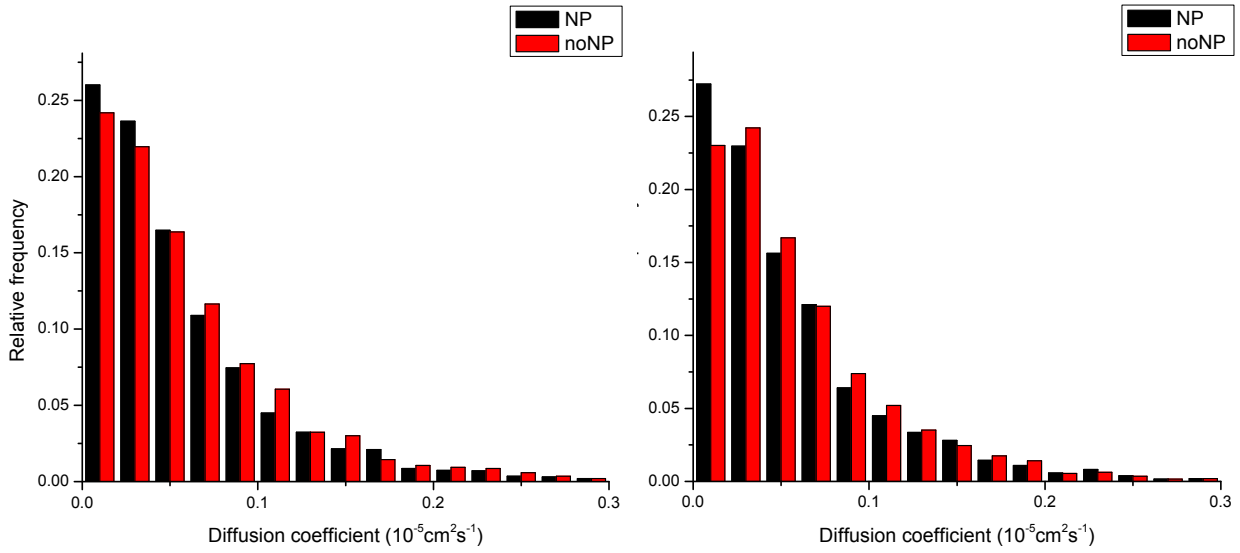

Figure 4.13: Distribution of the molecular diffusion coefficients in the POPC(left)/POPG(right) bilayer with (black columns) and without nanoparticles (red columns).

5 Conclusion and outlook

In this work coarse-grained simulations of membranes in the presence of gold nanoparticles have been performed to investigate the changes in the static and dynamic properties of the membranes. Lipid bilayers consisting of POPC, POPG and a mixture of the two lipids were chosen as membrane models. The representations and force field parameters from the MARTINI model were used in the simulations together with a recently developed MARTINI model of cationic and anionic alkylthiolate coated gold nanoparticles. Unbiased simulations of small and large membrane patches in water with different concentrations of nanoparticles have been performed. This made sure that no behavior and effects were artificially enforced. The results have been compared to other simulation studies as well as to experimental data as far as it was available.

The coarse-grained simulations were able to reproduce the results of many other coarse-grained but also of atomistic studies. The three simulated bilayers reproduced structural properties from experiments very well at simulation conditions. They were found to be tensionless and in a fluid state, as desired. An attachment of nanoparticles to these bilayers, guided by Coulomb interactions, was observed in systems with opposite charges, while nanoparticles carrying the same charge as the bilayer were repelled. Also an attachment mechanism, that featured a weaker, metastable intermediate and a final, stronger binding state was observed. This is in perfect agreement with other atomistic and coarse-grained simulations. The structures of the nanoparticles attached to the membrane were also similar to the ones obtained from atomistic simulations. This showed that the necessary interactions are considered in the model used in this work.

The density profiles of the lipid bilayers showed that the perturbation of the lipid structure due to attachment of cationic nanoparticles is stronger in membranes with a higher negative surface charge density. However, the nanoparticle influences only the lipid layer facing it, while the opposing layer is almost undistorted. This was also confirmed by the analysis of the lipid order in both layers close to and far away from the nanoparticles. It was also observed that the nanoparticles changed the local composition of the lipid layer they attached to, as the negative POPG has a much higher affinity to the cationic nanoparticles than the neutral POPC. This is also reflected in the behavior of the nanoparticles on the different bilayers. While the nanoparticles on the homogenous POPG bilayer were quasi equally distributed, they moved closer to each other on the mixed POPC/POPG bilayer, forming dynamic agglomerates.

The nanoparticles were found to globally reduce the diffusion in the lipid bilayers by formation of raft-like domains in the underlying lipid layer. In these domains the lipids diffuse together with the slower nanoparticle. However, there is a constant exchange with the surroundings of lipids entering and leaving the region close to the nanoparticle. This is the first actual confirmation of the mechanism for the hypothesis of enslaved diffusion. This hypothesis was a possible explanation of different lipid diffusion rates in the presence of gold nanoparticles, that have been observed in experiments.

Overall, the coarse-grained simulations performed in this work have proven to be very useful for the investigations of the interactions of gold nanoparticles and lipid bilayers. Not only did they show the desired behavior and were able to reproduce results of other simulations as well as experiments, they also showed not yet reported effects and provided new insights into the topic.

With these promising results there are a lot of possibilities for future investigations. A challenging task would be the quantitative correlation of the velocities and diffusion rates of the nanoparticles and the lipid molecules. In this context also the exchange rates of lipids in the raft-like domains could be investigated. Simulations with bigger and therefore slower nanoparticles could be interesting for these investigations, as they should increase the influence of the nanoparticle on the lipid diffusion. The influence of the nanoparticles on the undulations and the rigidity of the membrane has not been investigated in this work but is also possible with these kind of coarse-grained simluations. Further, it could be useful to switch from a particle-particle to a particle-field approach as even longer time and length scales may be necessary. At last the investigation of the influence of the nanoparticles on the structure and composition of membranes containing different lipids is very promising. This effect has only been slightly touched in this work, while it may be one of the most important factors in biological membranes that are built up of many different components. Ideally this future work would be accompanied by new experiments that are able to support the simulation results.

List of Figures

List of Tables

Bibliography

[1] William E. Doering and Shuming Nie. Spectroscopic tags using dye-embedded nanoparticles and surface-enhanced raman scattering. *Analytical chemistry*, 75(22):6171–6176, 2003.

[2] Feng Wang and Xiaogang Liu. Upconversion multicolor fine-tuning: visible to near-infrared emission from lanthanide-doped nayf4 nanoparticles. *Journal of the American Chemical Society*, 130(17):5642–5643, 2008.

[3] Joseph Kao, Kari Thorkelsson, Peter Bai, Benjamin J. Rancatore, and Ting Xu. Toward functional nanocomposites: taking the best of nanoparticles, polymers, and small molecules. *Chem. Soc. Rev.*, 42:2654–2678, 2013.

[4] Jens Rauch, Walter Kolch, Sophie Laurent, and Morteza Mahmoudi. Big signals from small particles: Regulation of cell signaling pathways by nanoparticles. *Chem. Rev.*, 113(5):3391–3406, 2013.

[5] James J. Storhoff, Robert Elghanian, Robert C. Mucic, Chad A. Mirkin, and Robert L. Letsinger. One-pot colorimetric differentiation of polynucleotides with single base imperfections using gold nanoparticle probes. *Journal of the American Chemical Society*, 120(9):1959–1964, 1998.

[6] Jyoti K. Jaiswal and Sanford M. Simon. Potentials and pitfalls of fluorescent quantum dots for biological imaging. *Trends in cell biology*, 14(9):497–504, 2004.

[7] Morteza Mahmoudi, Shilpa Sant, Ben Wang, Sophie Laurent, and Tapas Sen. Superparamagnetic iron oxide nanoparticles (spions): development, surface modification and applications in chemotherapy. *Advanced drug delivery reviews*, 63(1):24–46, 2011.

[8] James C. Y. Kah, John Chen, Angel Zubieta, and Kimberly Hamad-Schifferli. Exploiting the protein corona around gold nanorods for loading and triggered release. *ACS Nano*, 6(8):6730–6740, 2012.

[9] Christopher Loo, Amanda Lowery, Naomi Halas, Jennifer West, and Rebekah Drezek. Immunotargeted nanoshells for integrated cancer imaging and therapy. *Nano letters*, 5(4):709–711, 2005.

[10] Xiaohua Huang, Prashant K. Jain, Ivan H. El-Sayed, and Mostafa A. El-Sayed. Determination of the minimum temperature required for selective photothermal destruction of cancer cells with the use of immunotargeted gold nanoparticles. *Photochemistry and photobiology*, 82(2):412–417, 2006.

[11] Yu Pan, Sabine Neuss, Annika Leifert, Monika Fischler, Fei Wen, Ulrich Simon, Günter Schmid, Wolfgang Brandau, and Willi Jahnen-Dechent. Size-dependent cytotoxicity of gold nanoparticles. *Small*, 3(11):1941–1949, 2007.

[12] Devika B. Chithrani, Arezou A. Ghazani, and Warren C. W. Chan. Determining the size and shape dependence of gold nanoparticle uptake into mammalian cells. *Nano Lett.*, 6(4):662–668, 2006.

[13] Anna Lesniak, Anna Salvati, Maria J. Santos-Martinez, Marek W. Radomski, Kenneth A. Dawson, and Christoffer Aberg. Nanoparticle adhesion to the cell membrane and its effect on nanoparticle uptake efficiency. *J. Am. Chem. Soc.*, 135(4):1438–1444, 2013.

[14] Francesco Stellacci, Randy P. Carney, Reid C. Van Lehn, Darrell J. Irvine, Alfredo Alexander-Katz, Yu-Sang Yang, and Prabhani U. Atukorale. Effect of Particle Diameter and Surface Composition on the Spontaneous Fusion of Monolayer-Protected Gold Nanoparticles with Lipid Bilayers. *Nano Lett.*, 13(9):4060–4067, 2013.

[15] Shengwen Zhang, Andrew Nelson, and Paul A. Beales. Freezing or wrapping: The role of particle size in the mechanism of nanoparticle biomembrane interaction. *Langmuir*, 28(35):12831–12837, 2012.

[16] Ayush Verma, Oktay Uzun, Yuhua Hu, Ying Hu, Hee-Sun Han, Nicki Watson, Suelin Chen, Darrell J. Irvine, and Francesco Stellacci. Surface-structure-regulated cell-membrane penetration by monolayer-protected nanoparticles. *Nat. Mater.*, 7(7):588–595, 2008.

[17] Costanza Montis, Daniele Maiolo, Ivano Alessandri, Paolo Bergese, and Debora Berti. Interaction of nanoparticles with lipid membranes: a multiscale perspective. *Nanoscale*, 6:6452–6457, 2014.

[18] Arthur A. Spector and Mark A. Yorek. Membrane lipid composition and cellular function. *Journal of lipid research*, 26(9):1015–1035, 1985.

[19] Angelikopoulos P. Homogeneous hydrophobic–hydrophilic Surface Patterns enhance Permeation of Nanoparticles through Lipid Membranes. *J. Phys. Chem. Lett.*, 4:1907, 2013.

[20] Paraskevi Gkeka, Panagiotis Angelikopoulos, Lev Sarkisov, and Zoe Cournia. Membrane Partitioning of Anionic, Ligand-Coated Nanoparticles Is Accompanied by Ligand Snorkeling, Local Disordering, and Cholesterol Depletion. *PLoS Comput. Biol.*, 10(12), 2014.

[21] Federica Simonelli, Davide Bochicchio, Riccardo Ferrando, and Giulia Rossi. Monolayer-Protected Anionic Au Nanoparticles Walk into Lipid Membranes Step by Step. *J. Phys. Chem. Lett.*, 6(16):3175–3179, 2015.

[22] Elena Heikkilä, Hector Martinez-Seara, Andrey A. Gurtovenko, Matti Javanainen, Hannu Häkkinen, Ilpo Vattulainen, and Jaakko Akola. Cationic Au nanoparticle binding with plasma membrane-like lipid bilayers: Potential mechanism for spontaneous permeation to cells revealed by atomistic simulations. *J. Phys. Chem. C*, 118(20):11131–11141, 2014.

[23] Elena Heikkilä, Hector Martinez-Seara, Andrey A. Gurtovenko, Ilpo Vattulainen, and Jaakko Akola. Atomistic simulations of anionic Au144(SR)60 nanoparticles interacting with asymmetric model lipid membranes. *Biochim. Biophys. Acta - Biomembr.*, 1838(11):2852–2860, 2014.

[24] Anil R. Mhashal and Sudip Roy. Effect of gold nanoparticle on structure and fluidity of lipid membrane. *PLoS One*, 9(12):1–18, 2014.

[25] Jiaqi Lin, Hongwu Zhang, Zhen Chen, and Yonggang Zheng. Penetration of lipid membranes by gold nanoparticles: insights into cellular uptake, cytotoxicity, and their relationship. *ACS nano*, 4(9):5421–5429, 2010.

[26] Jia Qi Lin, Yong Gang Zheng, Hong Wu Zhang, and Zhen Chen. A simulation study on nanoscale holes generated by gold nanoparticles on negative lipid bilayers. *Langmuir*, 27(13):8323–8332, 2011.

[27] Jiaqi Lin and Alfredo Alexander-katz. Cell Membranes Open "Doors" for Cationic Nanoparticles / Biomolecules : Insights into Uptake Kinetics. *ACS Nano*, 7(12):10799–10808, 2013.

[28] Emily M. Curtis, Amir H. Bahrami, Thomas R. Weikl, and Carol K. Hall. Modeling nanoparticle wrapping or translocation in bilayer membranes. *Nanoscale*, 7(34):14505–14514, 2015.

[29] Falin Tian, Tongtao Yue, Ye Li, and Xianren Zhang. Computer simulation studies on the interactions between nanoparticles and cell membrane. *Sci. China Chem.*, 57(12):1662–1671, 2014.

[30] Siewert J. Marrink, Alex H. De Vries, and Alan E. Mark. Coarse grained model for semiquantitative lipid simulations. *J. Phys. Chem. B*, (108):750–760, 2004.

[31] Siewert J. Marrink, Jelger H. Risselada, Serge Yefimov, Peter D. Tieleman, and Alex H. De Vries. The MARTINI force field: Coarse grained model for biomolecular simulations. *J. Phys. Chem. B*, 111(27):7812–7824, 2007.

[32] Robert D. Groot and KL Rabone. Mesoscopic simulation of cell membrane damage, morphology change and rupture by nonionic surfactants. *Biophysical journal*, 81(2):725–736, 2001.

[33] D.R. Lide. *CRC Handbook of Chemistry and Physics: A Ready-reference Book of Chemical and Physical Data*. CRC-Press, 1995.

[34] Giuseppe Milano, G. Santangelo, F. Ragone, L. Cavallo, and A. Di Matteo. Gold nanoparticle/polymer interfaces: All atom structures from molecular dynamics simulations. *J. Phys. Chem. C*, 115(31):15154–15163, 2011.

[35] Kai Simons and Winchil L. C. Vaz. Model systems, lipid rafts, and cell membranes 1. *Annu. Rev. Biophys. Biomol. Struct.*, 33:269–295, 2004.

[36] Svetlana Baoukina, Luca Monticelli, Jelger H. Risselada, Siewert J. Marrink, and Peter D. Tieleman. The molecular mechanism of lipid monolayer collapse. *Proceedings of the National Academy of Sciences*, 105(31):10803–10808, 2008.

[37] Tsjerk A. Wassenaar, Helgi I. Ingólfsson, Rainer A. Böckmann, Peter D. Tieleman, and Siewert J. Marrink. Computational lipidomics with insane: a versatile tool for generating custom membranes for molecular simulations. *Journal of chemical theory and computation*, 11(5):2144–2155, 2015.

[38] Herman J. C. Berendsen, David van der Spoel, and Rudi van Drunen. GROMACS: A message-passing parallel molecular dynamics implementation. *Comp. Phys. Comm.*, 91:43–56, 1995.

[39] Erik Lindahl, Berk Hess, and David van der Spoel. GROMACS 3.0: A package for molecular simulation and trajectory analysis. *J. Mol. Mod.*, 7:306–317, 2001.

[40] David van der Spoel, Erik Lindahl, Berk Hess, Gerrit Groenhof, Alan E. Mark, and Herman J. C. Berendsen. GROMACS: Fast, Flexible and Free. *J. Comp. Chem.*, 26:1701–1719, 2005.

[41] Berk Hess, Carsten Kutzner, David van der Spoel, and Erik Lindahl. GROMACS 4: Algorithms for highly efficient, load-balanced, and scalable molecular simulation. *J. Chem. Theory Comput.*, 4:435–447, 2008.

[42] Sander Pronk, Szilárd Páll, Roland Schulz, Per Larsson, Pär Bjelkmar, Rossen Apostolov, Micheal R. Shirts, Jeremy C. Smith, Peter M. Kasson, David van der Spoel, Berk Hess, and Erik Lindahl. GROMACS 4.5: a high-throughput and highly parallel open source molecular simulation toolkit. *Bioinformatics*, 29:845–854, 2013.

[43] Szilárd Páll, Mark James Abraham, Carsten Kutzner, Berk Hess, and Erik Lindahl. Tackling Exascale Software Challenges in Molecular Dynamics Simulations with GROMACS. *Solving Software Challenges for Exascale*, 8759:3–27, 2015.

[44] Mark James Abraham, Teemu Murtola, Roland Schulz, Szilárd Páll, Jeremy C. Smith, Berk Hess, and Erik Lindahl. GROMACS: High performance molecular simulations through multi-level parallelism from laptops to supercomputers. *SoftwareX*, 1:19–25, 2015.

[45] L. Martínez, R. Andrade, E. G. Birgin, and J. M. Martínez. Packmol : A package for building initial configurations for molecular dynamics simulations. 2008.

[46] William Humphrey, Andrew Dalke, and Klaus Schulten. Vmd: visual molecular dynamics. *Journal of molecular graphics*, 14(1):33–38, 1996.

[47] Norbert Kučerka, Mu-Ping Nieh, and John Katsaras. Fluid phase lipid areas and bilayer thicknesses of commonly used phosphatidylcholines as a function of temperature. *Biochimica et Biophysica Acta (BBA) - Biomembranes*, 1808(11):2761 – 2771, 2011.

[48] Jianjun Pan, Frederick A Heberle, Stephanie Tristram-Nagle, Michelle Szymanski, Mary Koepfinger, John Katsaras, and Norbert Kučerka. Molecular structures of fluid phase phosphatidylglycerol bilayers as determined by small angle neutron and X-ray scattering. *Biochim. Biophys. Acta*, 1818(9):2135–48, 2012.

[49] The GROMACS development teams at the Royal Institute of Technology and Uppsala University. *GROMACS user manual 5.0.7*, 2015.

Appendix

I. Simulation snapshots: enslaved diffusion

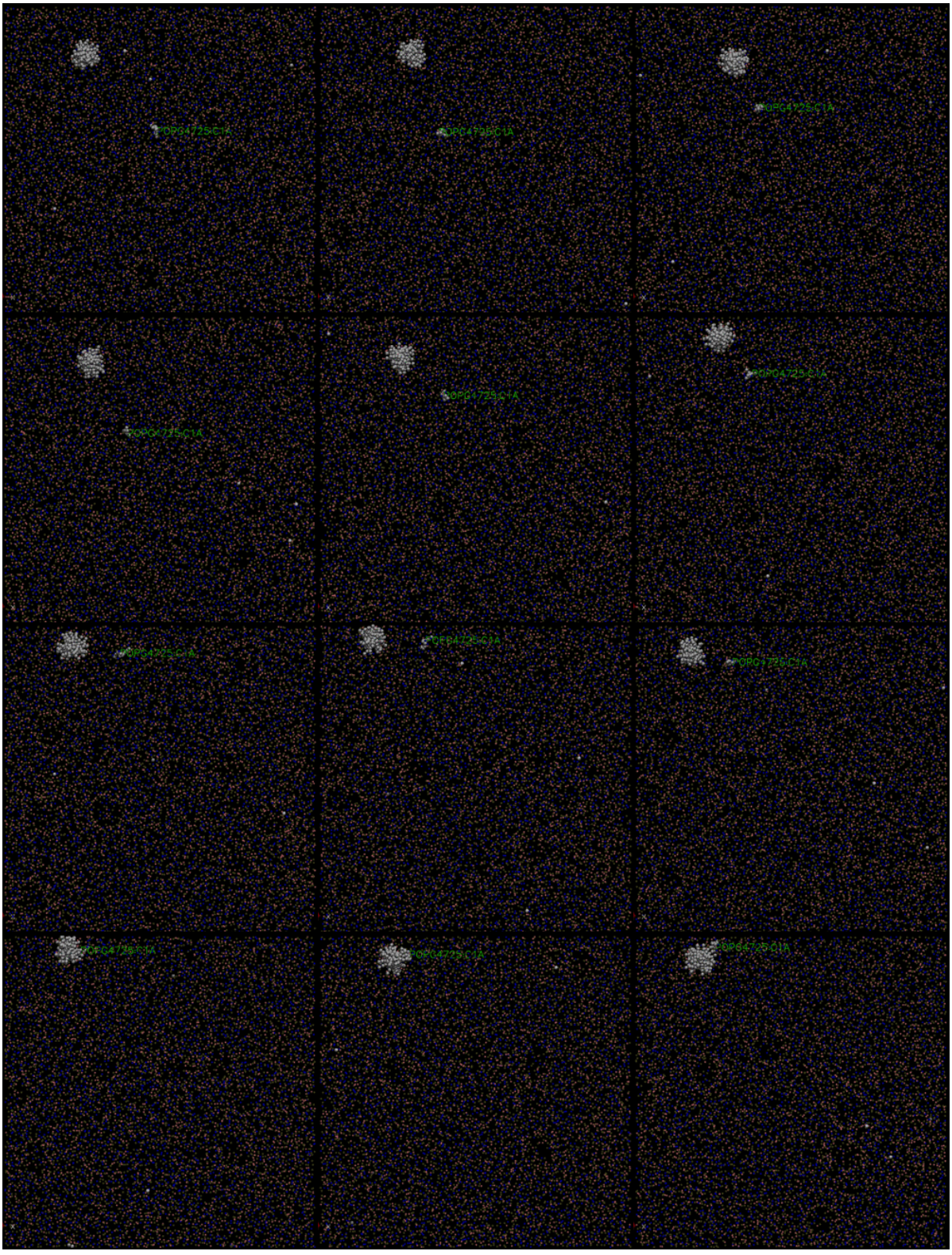

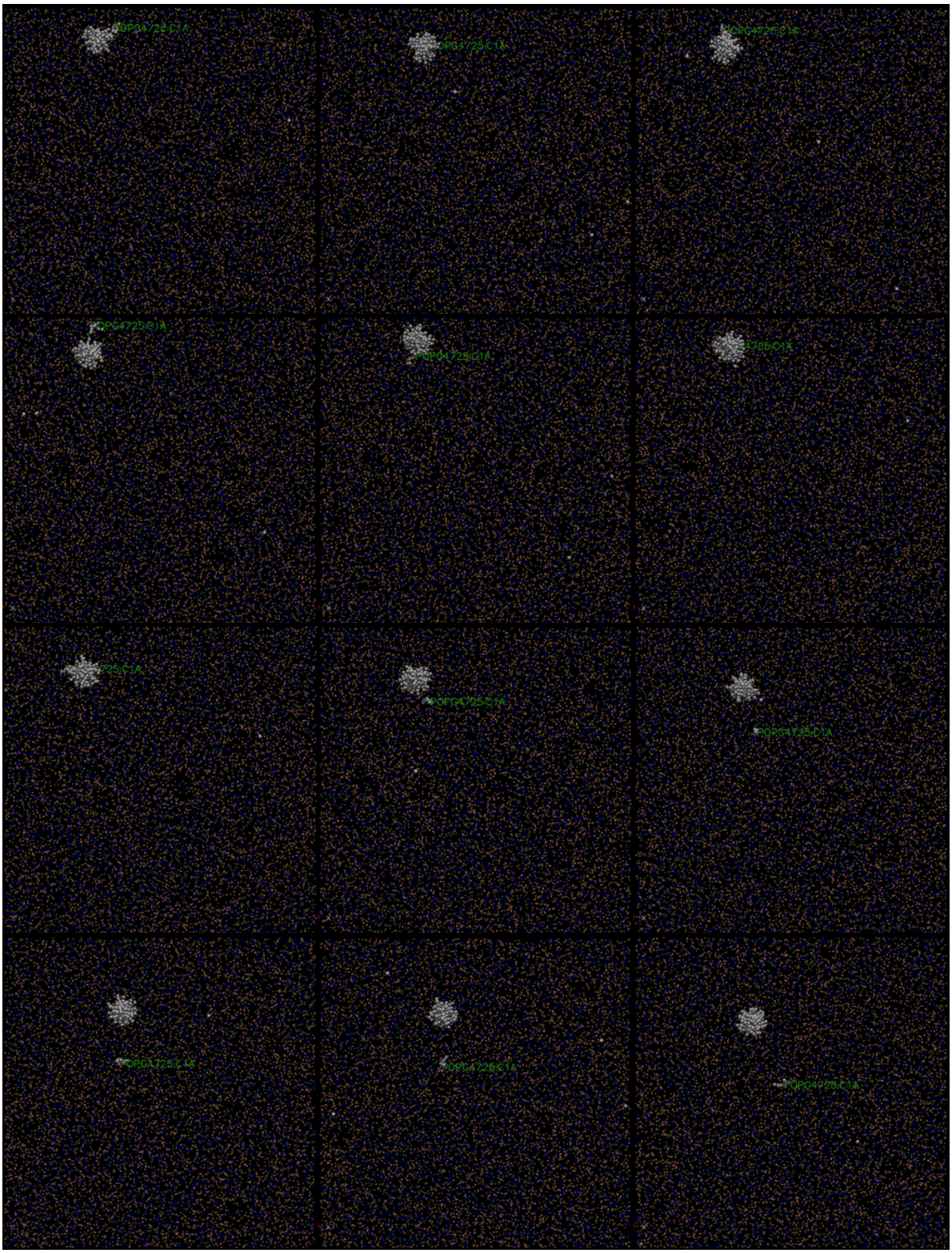

Simulation snapshots of the mixed bilayer in top view. One of the 16 nanoparticles and one lipid are highlighted in gray. Frames are ordered in time, left to right and top to bottom. The two molecules diffuse freely (frames 1-9) and when they meet (10) they diffuse together (11-19). After some time they separate (frame 20) and diffuse independently again.

II. Program code: localorder.cpp

```
/*
 Custom Analysis Tool for GROMACS (v5.1.1)
 Written by Tobias Pfeiffer February 2016 using the template for Analysis Tools
 */

#include <string>
#include <vector>
#include <gromacs/trajectoryanalysis.h> //      make sure GMXRC is sourced or
                                        //      adjust path to trajectoryananlysis.h
#include <fstream>
#include <iomanip>
#include <iostream>

using namespace gmx;

real       averageorder = 0.0;  // global variables with scope
int         framenumber = 0;    // beyond frame level

/*! \brief
 * Template class to serve as a basis for user analysis tools.
 */
class AnalysisTemplate : public TrajectoryAnalysisModule
{
public:
    AnalysisTemplate();

    virtual void initOptions(Options                    *options,
                             TrajectoryAnalysisSettings *settings);
    virtual void initAnalysis(const TrajectoryAnalysisSettings &settings,
                              const TopologyInformation        &top);

    virtual void analyzeFrame(int frnr, const t_trxframe &fr, t_pbc *pbc,
                              TrajectoryAnalysisModuleData *pdata);

    virtual void finishAnalysis(int nframes);
    virtual void writeOutput();

private:
    class ModuleData;

    std::string                      fnDist_;
    double                           cutoff_;
    Selection                        refsel_;
    SelectionList                    sel_;

    AnalysisNeighborhood             nb_;

    AnalysisData                     data_;
    AnalysisDataAverageModulePointer avem_;
    std::ofstream                    ofs_;
};


AnalysisTemplate::AnalysisTemplate()
: TrajectoryAnalysisModule("template", "Template analysis tool"),
```

```
cutoff_(0.0)
{
    registerAnalysisDataset(&data_, "avedist");
}


void
AnalysisTemplate::initOptions(Options                    *options,
                              TrajectoryAnalysisSettings *settings)
{
    static const char *const desc[] = {
        "This is a module for the calculation of the composition",
        "as a function of the three carthesian coordinates",
        "A reference group is selected. The module calculates the",
        "distance of all positions in the selection(s) from all the ",
        "positions in the reference group in every frame and writes ",
        "them to the output file."};

    options->setDescription(desc);

    options->addOption(FileNameOption("o")
                       .filetype(eftPlot).outputFile()
                       .store(&fnDist_).defaultBasename("avedist")
                       .description("order parameter"));

    options->addOption(SelectionOption("reference")
                       .store(&refsel_).required()
                       .description("Reference group to calculate distances from"));
    options->addOption(SelectionOption("select")
                       .storeVector(&sel_).required().multiValue()
                       .description("Groups to calculate distances to"));

    settings->setFlag(TrajectoryAnalysisSettings::efRequireTop);
}


void
AnalysisTemplate::initAnalysis(const TrajectoryAnalysisSettings &settings,
                               const TopologyInformation        & /*top*/)
{
    std::ofstream oldfile;
    oldfile.open("localorder.dat",  std::ofstream::trunc);
    oldfile.close();
    data_.setColumnCount(0, sel_.size());
}

// this function is called for each frame in the trajectory
void
AnalysisTemplate::analyzeFrame(int frnr, const t_trxframe &fr, t_pbc *pbc,
                               TrajectoryAnalysisModuleData *pdata)
{
    AnalysisDataHandle         dh     = pdata->dataHandle(data_);
    const Selection           &refsel = pdata->parallelSelection(refsel_);

    dh.startFrame(frnr, fr.time); // Start data for new frame

    std::ofstream fs;
    fs.open("localorder.dat",  std::ofstream::app);    // opens output file
```

```
    for (size_t g = 0; g < sel_.size(); ++g)
    {
        const Selection &sel   = pdata->parallelSelection(sel_[g]);
                  // adds selection to the module data for the frame
        int              selnr    = sel.posCount();  //return numbers of
        int              refnr    = refsel.posCount();  // positions in the selections

        if(selnr != refnr){return;}  //check if selections are consistent

        real             x = 0.0;              //  coordinates
        real             y = 0.0;              // of the lipid
        real             z = 0.0;              // orientation vector
        real             theta = 0.0;
        real             theta2 = 0.0;
        real             absolute = 0.0;
        real             sz = 0.0;
        real             averagetheta2  = 0.0;
        int              counter = 0;    // keeps track of the number of positions
                //  for the calculation of averagetheta

        for (int i = 0; i < selnr; ++i)    // loop over all positions in the selection
        {

                SelectionPosition selp = sel.position(i);  // Accesse a single position
                 SelectionPosition refp = refsel.position(i); //  in the selections

                x = selp.x()[0]-refp.x()[0];    //calculation of the x-
                y = selp.x()[1]-refp.x()[1];    //y-
                z = selp.x()[2]-refp.x()[2];    //and z-component of the lipid vector

                absolute = sqrt(x*x+y*y+z*z);      // calculates vector length "absolute"
                theta = z/absolute;             // this actually calculates cos(theta)
                theta2 = theta*theta;           // squarinf of theta

                averagetheta2 = (averagetheta2 * counter + theta2)/(counter+1);
                 // updating the frame average
                counter++;        // counter increment
        }

        sz = 1.5*averagetheta2 - 0.5;   // calculates order parameter sz
        fs.precision(5);
        fs.width(10);
        fs  << sz << std::endl;         // writes frame average to output file

        averageorder = (averageorder * framenumber + sz)/(framenumber+1);
        // updating the average over all frames
        framenumber++;                  // framenumber increment

    }
    dh.finishFrame();       // finishes data handel for this frame
}


void
AnalysisTemplate::finishAnalysis(int /*nframes*/)
{
```

```
    // writing average order from all frames to output file
    std::ofstream fs;
    fs.open("localorder.dat",  std::ofstream::app);
    fs  << "Average over " << framenumber << " frames:\t"
                << averageorder << std::endl;
}


void
AnalysisTemplate::writeOutput()
{
    // Message at the end of the analysis
    fprintf(stderr, "Finished successfully!\n");
}

/*! \brief
 * The main function for the analysis template.
 */
int
main(int argc, char *argv[])
{
return gmx::TrajectoryAnalysisCommandLineRunner::runAsMain<AnalysisTemplate>(argc,argv);
}
```

III. Program code: frations.cpp

```
/*
 Custom Analysis Tool for GROMACS (v5.1.1)
Written by Tobias Pfeiffer March 2016 using the template for Analysis Tools
 */

#include <string>
#include <vector>
#include <gromacs/trajectoryanalysis.h>
#include <fstream>
#include <iomanip>
#include <iostream>

using namespace gmx;

//global variables
int i;
int refcount = 0;
int validframes[304];
int molcount = 0;
double fraction = 0.0;

/*! \brief
 * Template class to serve as a basis for user analysis tools.
 */
class AnalysisTemplate : public TrajectoryAnalysisModule
{
public:
    AnalysisTemplate();

    virtual void initOptions(Options                    *options,
                             TrajectoryAnalysisSettings *settings);
    virtual void initAnalysis(const TrajectoryAnalysisSettings &settings,
                              const TopologyInformation        &top);

    virtual void analyzeFrame(int frnr, const t_trxframe &fr, t_pbc *pbc,
                              TrajectoryAnalysisModuleData *pdata);

    virtual void finishAnalysis(int nframes);
    virtual void writeOutput();

private:
    class ModuleData;

    std::string                     fnDist_;
    double                          cutoff_;
    Selection                       refsel_;
    SelectionList                   sel_;

    AnalysisNeighborhood            nb_;

    AnalysisData                    data_;
    AnalysisDataAverageModulePointer avem_;
    std::ofstream                   ofs_;
};
```

```
AnalysisTemplate::AnalysisTemplate()
: TrajectoryAnalysisModule("template", "Template analysis tool"),
cutoff_(0.0)
{
    registerAnalysisDataset(&data_, "avedist");
}


void
AnalysisTemplate::initOptions(Options                    *options,
                              TrajectoryAnalysisSettings *settings)
{
    static const char *const desc[] = {
        "This is a module for the calculation of the time fraction"
        "that a position spends close to another position in a simulation",
        "A reference group (lipids) is selected. The module calculates the",
        "distance of all positions in the selection(s) (NPs) from all the ",
        "positions in the reference group in every frame and writes ",
        "them to the output file."};

    options->setDescription(desc);

    options->addOption(FileNameOption("o")
                       .filetype(eftPlot).outputFile()
                       .store(&fnDist_).defaultBasename("avedist")
                       .description("Average distances from reference group"));

    options->addOption(SelectionOption("reference")
                       .store(&refsel_).required()
                       .description("Reference group to calculate distances from"));
    options->addOption(SelectionOption("select")
                       .storeVector(&sel_).required().multiValue()
                       .description("Groups to calculate distances to"));

    settings->setFlag(TrajectoryAnalysisSettings::efRequireTop);
}

void
AnalysisTemplate::initAnalysis(const TrajectoryAnalysisSettings &settings,
                               const TopologyInformation         & /*top*/)
{

    std::ofstream oldfile;  //opening output file
    oldfile.open("fractions.dat",  std::ofstream::trunc);
    oldfile.close();

    for(i=0;i<304;i++){

        validframes[i] = 0;

    } //Initialization of the Array

    data_.setColumnCount(0, sel_.size());
}

// this function is called for each frame in the trajectory
void
AnalysisTemplate::analyzeFrame(int frnr, const t_trxframe &fr, t_pbc *pbc,
```

```
                                TrajectoryAnalysisModuleData *pdata)
{
    AnalysisDataHandle         dh     = pdata->dataHandle(data_);
    const Selection           &refsel = pdata->parallelSelection(refsel_);
    //  initializes reference selection
    int                        refnr    = refsel.posCount();
    //  returns number of positions in the selection

    dh.startFrame(frnr, fr.time); // Start data for new frame

    real             xdist = 0.0;
    real             ydist = 0.0;
    real             xydist2 = 0.0;
    real             zdist = 0.0;

    for (size_t g = 0; g < sel_.size(); ++g)
    {
        const Selection &sel   = pdata->parallelSelection(sel_[g]);
        int              selnr    = sel.posCount();
        //      returns number of positions in the selection


        for (int i = 0; i < refnr; ++i)
        {

            for (int j = 0; j < selnr; ++j)
            {

                SelectionPosition refp = refsel.position(i); // Accesse a single
                SelectionPosition selp = sel.position(j);  // position the selections

                xdist = selp.x()[0]-refp.x()[0];    //calculation of the x-
                ydist = selp.x()[1]-refp.x()[1];    //y-
                zdist = selp.x()[2]-refp.x()[2];    //and z-distance

                xydist2 = xdist*xdist + ydist*ydist; //calculation of xy-dist

                if(zdist < 2.65 && xydist2 < 4){ //check for closeness to reference
                    validframes[i] += 1;
                }

            }
        }


    }
    refcount++;
    dh.finishFrame();  // finishing of data handle for frame
}

void
AnalysisTemplate::finishAnalysis(int /*nframes*/)
{
}

void
AnalysisTemplate::writeOutput()
{
```

```
    std::ofstream fs;   //opening output file
    fs.open("fractions.dat",  std::ofstream::app);

    for(i=0;i<304;i++){

            fraction = validframes[i];
            fraction /= refcount;
            fs.precision(5);
            fs.width(7);
            fs  << i;
            fs.precision(5);
            fs.width(8);
            fs  << validframes[i];
            fs.precision(5);
            fs.width(12);
            fs  << fraction << std::endl;
    } //write output to output file

    fprintf(stderr, "Finished successfully!\n");
}

/*! \brief
 * The main function for the analysis template.
 */
int
main(int argc, char *argv[])
{
 return gmx::TrajectoryAnalysisCommandLineRunner::runAsMain<AnalysisTemplate>(argc, argv);
}
```